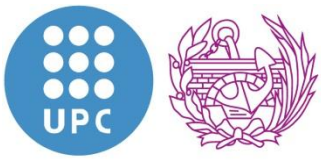

Escola Tècnica Superior d'Enginyers de Camins, Canals i Ports de Barcelona

UNIVERSITAT POLITÈCNICA DE CATALUNYA

PROJECTE O TESINA D'ESPECIALITAT

Títol

MICROSTRUCTURE AND ITS EFFECTS ON COMPACTION IN BARCELONA SILTY-CLAYS

Autor/a

VITA SANDERSON

Tutor/a

EDUARDO ALONSO

Departament

ENGINYERIA DEL TERRENY

Data

BARCELONA, JUNY 2011

Agradecimientos

Gracias a Eduardo Alonso, tutor de esta tesina y a Enrique Romero y Josep Suriol para toda sus ayuda durante los últimos 6 meses.

A José y Victor para su ayuda en el laboratorio. Y especialmente a Rodrigo, sin tu ayuda, ¡nada de esto hubiera sido posible!

Resumen

Los recientes avances en la caracterización de los suelos no saturados han permitido el desarrollo de modelos constitutivos de la conducta de estos suelos. Estudios previos han mostrado las tendencias del hinchamiento y el potencial de colapso de los suelos sometidos a camino de humedecimiento y secado. El objetivo de este estudio es investigar los cambios que los efectos en el rendimiento de la humedad sobre el comportamiento de los suelos parcialmente saturados en condiciones de deformación volumétrica a cero.

El uso de datos porosimetricos se utilizarán para caracterizar los cambios en la microestructura, mientras que un programa experimental de ensayos de succión controlada edométrico y pruebas de resonancia columna investigar los cambios en las características de comportamiento en el suelo.

Abstract

Recent advances in the characterization of unsaturated soils have allowed the development of constitutive models of the behaviour of these soils. Previous studies have shown the trends in the swelling and collapse potential of soils subjected to wetting and drying paths. The aim of this study is to investigate what effects changes in humidity yield on the behaviour of partially saturated soil under conditions of zero volumetric strain.

The use of porosimetric data will be used to characterize changes in microstructure whilst an experimental program of suction controlled oedometer tests and resonant column tests will investigate changes in behavioural characteristics in the soil.

Table of Contents

List of Figures

1. Chapter 1 – INTRODUCTION

1.1. Introduction

The behaviour during compaction of soil is of interest due to its applicability in the construction of dams, roadways and other civil and infrastructure projects. The behaviour of a plastic soil during compaction has been the focus of many investigations from as early as Proctor's fundamental principle of soil compaction (1933) and continues today to be the subject of much research around the world. Previous studies by Gens et al. (1995) show how the initial state of a soil at the time of compaction plays an integral role in its behaviour during and after compaction.

1.2. Structure of the document

Chapter 2 is literature study and summary of current state of knowledge within the field of compaction and the various lines of research that have been conducted. It is a study of the theory behind the behaviour of the soil with respect to the microstructure and the initial state of the soil when compacted. This will provide a context for the experimental program described in chapter 3 and give a broader understanding of the effects that affect the behaviour of soils in compaction as presented in the results in chapter 4. Summarising remarks and conclusions are in chapter 5 followed by possible further lines of investigation.

1.3. Objectives and Methodology

The aim of this investigation is study the effects that differences in compaction conditions, specifically water content, have on the structure and behaviour of the soil. By completing a varied range of tests, the aim is to gain a more complete picture of the changes that occur within the microstructure during and wetting and drying and their effect on the behaviour of the soil.

1.4. Testing Program

Experiment	Samples Tested
Standard Proctor	Dry side: 6.3%,7.6%,9.2%
	Wet side: 10.1%, 11.6%, 13.9%
Modified Proctor	Dry side: 5.8%, 7.1%
	Wet side: 8.6%, 9.2%
Static Compaction	Dry side: 12.5%
Mercury Intrusion Porosimetry	DD, DW, WD, WW
WP4 Dew-Point Potentiometer	DD, WW
Suction Controlled Oedometer	DD-20kPa, DD-400kPa, WD-400kPa
Resonant Column	DD, DW, WD, WW

1.5. Origin of the soil

The soil is a red silty-clay found naturally in Barcelona, this particular sample is from the grounds of the university, Campus Nord. The tests were conducted on artificially constructed samples made from the clay powder, not in their naturally occurring state. It is similar to soil used in the development of the Barcelona Basic Model (Alonso et al., 1990)

2. Chapter 2 – CURRENT STATE OF KNOWLEDGE

2.1. A Brief History of Developments in Partially Saturated Soils

Whilst saturated soils are very well understood and modelled, the field of unsaturated or partially soil is much less comprehensively investigated. Moreover, the scope within the field of partially saturated soils is much broader with many variables that must be accounted for, with great diversity in the type and behaviour of soils. These were initially treated as “special problem soils” (Alonso et al., 1987) followed by the development of a model, the Barcelona Basic Model (Alonso et al., 1990).

Developments into the mechanics of unsaturated soils start with the development pore water tension maps (Lambe, 1959) and investigations into the validity of the effective stress concept in unsaturated soils (Aitchison and Bishop, 1960; Bishop and Blight, 1963). The concept was then modified for partially saturated soils however from 1965, research demonstrating the use of two stress variables was developed (Matyas and Radhakrishna, 1968; Fredlund, 1979) and concepts of net stress (total stress less air pressure) and suction (air pressure less pore water pressure) were introduced.

However, these models did not cover comprehensively the stress-strain response of partially saturated soils. Alonso et al. (1990) developed an elastoplastic hardening model describing the effect of suction changes on stiffness and reversibility of effects causes by stress and suction reversals.

The advent of techniques such as mercury intrusion porosimetry and the scanning electron microscope have allowed the earlier models of structure of Booth (1977) and Lambe (1958) to be revised and a more accurate picture of the microstructure of unsaturated soils and the differences between wet and dry side behaviour and developments in constitutive modelling over last decade (Tarantino, 2007; Sivakumar et al., 2010) have increased understanding of the behaviour of unsaturated soils.

2.2. Structure of the Soil

A soil sample can be divided up into 3 phases: air, water and solid as shown in Figure 2.1. In a fully saturated soil, there is no air phase as all the available space between soil particles is taken up by water, however in a partially saturated soil both the air and water phases are present and the effect of both of these must be taken into account when predicting and analysing unsaturated soil behaviour.

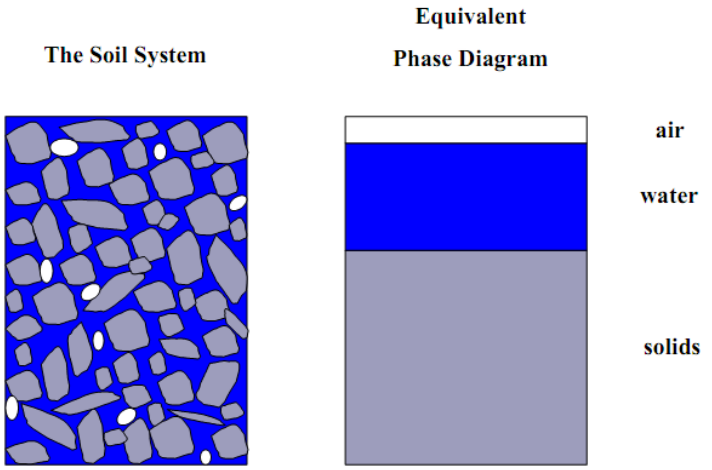

Figure 2.1: Diagram shows phase relationships of a soil (Mills and Cameron, 2002)

In simplified form, the internal structure of the soil can be accounted for in three types of elements (Alonso et al., 1987) which are elementary particles, aggregate particles and pores. From these elements, three fundamental structures can be established. These are a matrix type structure as shown in Figure 2.2(a) where the elementary clay particles are evenly distributed around sand grains in an array. Alternatively, the elementary clay particles are grouped like a grain of a larger size, this is a microstructure of aggregates Figure 2.2(b). Finally, it can be considered that the sand grains have either clay particle connectors between them or have direct contact, Figure 2.2(b).

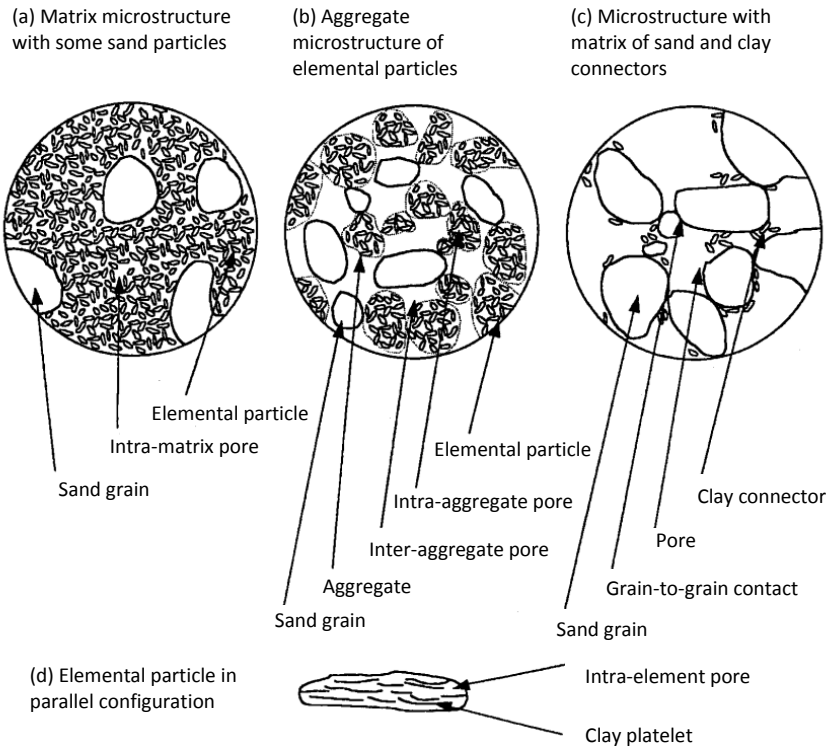

Figure 2.2: Soil Structure (adapted from Alonso et al., 1987)

2.3. Compacted Soils

Barden (1974) proposed that the optimum water content served as a good dividing line between wet and dry consolidation processes. Generally, soil compacted wet of optimum and expansive soils predominantly have a matric microstructure whereas soils compacted on the dry side of optimum, or those with a tendency to collapse often present microstructure of aggregates or with clay connectors (Alonso et al., 1987). When loading a soil with a microstructure of aggregates, the contacts between the aggregates or grains of sand are broken causing the aggregates to move into the space of the pores causing collapse. This behaviour is controlled by matric suction which works in two modes: the capillary component which is associated with the water between the aggregates, increases the stiffness of the structure when there is high suction and the adsorptive component, associated with the clay particles, maintains a low compressibility of the particles. Similarly, wetting the soil causes a decrease in the suction decreasing the resistance of the contact between aggregates causing collapse. Porosimetry studies shows the bimodal distribution of pores detected in the case of aggregated structures with the existence of inter-aggregate pores.

(a)

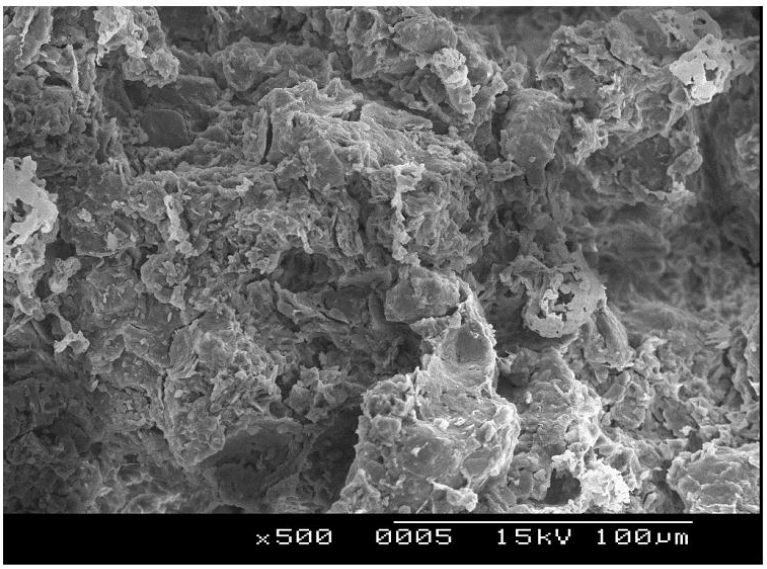

(b)

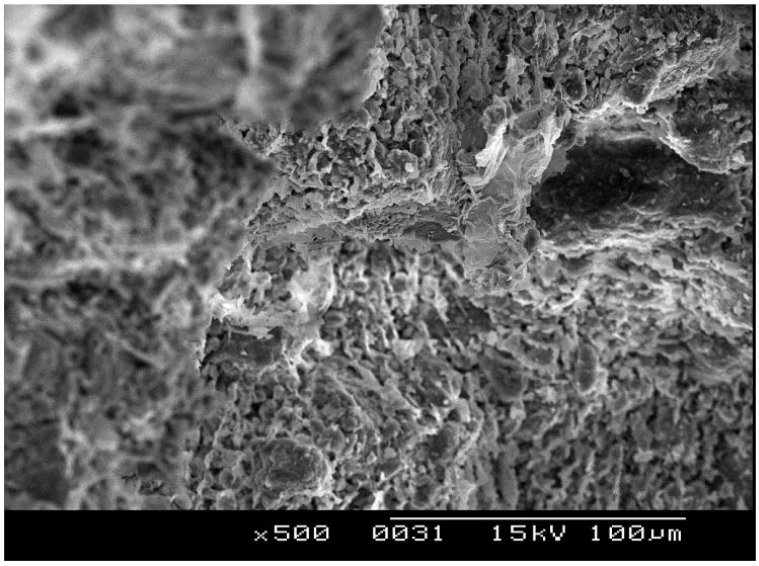

Figure 2.3: SEM photos showing differences in microstructure between samples compacted (a) dry of optimum and (b) wet of optimum (Alonso, 2007)

In Figure 2.3 are two scanning electron microscope photos of Barcelona silty-clay (similar to that used in this study) showing statically compacted samples on compacted on both the dry and the wet side of optimum. In part (a) you can see the existence of large pore between aggregates formed by stacking layers of clay of a smaller size (Alonso, 2007). In the photo (b), the structure is more uniform and the large pore that are apparent the in the soil compacted on the dry side do not appear.

Studies of soil compacted wet and dry of optimum show in general, that samples compacted on the dry side show a “bi-modal” PSD with two distinct peaks for fines and aggregates whereas those compacted on the wet side show a PSD with a single, wider peak (Barden and Sides, 1970, Gens et al., 1995) although often with a slight dip in the centre of the peak and that the differences in

behaviour of test specimens during compaction of each is due almost entirely to this phenomenon (Gens et al., 1995). Gens et al. (1995) proposed that these differences in behaviour could be attributed to two separate causes: microstructural or fabric differences and differences in suction prior to wetting and used suction controlled equipment to demonstrate the effect of structure on volume change.

We can define the initial state of a compacted soil by:

- Initial state of stress
- Initial density
- Initial parameters of the chosen constitutive model of soil behaviour (Alonso, 2007)

2.4. Suction in Unsaturated Soils

As mentioned above, matric suction is the effect of capillary action and adsorption of water in the soil. On evaporation of water from a soil's surface, the capillary menisci retreat into the soil voids and the "contractile skin" of surface tension forces exert a compressive stress on the soil skeleton. This stiffening effect is commonly found in soils in arid and semi-arid regions.

2.4.1. Techniques of Controlling Suction

Initial studies such as Booth's investigation on collapse settlement in road embankments (1977) and Barden (1974) were conducted without the benefit of the section controlling technology available today. Following that, Gens et al. (1995) showed using the suction-controlled oedometer and axis translation techniques how behaviour samples compacted dry and wet of optimum display significant differences in behaviour and structure.

2.4.2. Axis translation

Traditionally tensiometer measurements of matric suction were limited to 80kPa, however axis translation is a technique used to measure matric suction involving the translation of the reference pore air pressure (Delage et al., 2008), i.e. by artificially raising the atmospheric pressure around the sample (Marinho et al., 2006). In Figure 2.4 (a) we can see the typical case where the pore is subjected to atmospheric air pressure and in Figure 2.4 (b) we can see the results if the pore was subjected to elevated air pressure such as created in the laboratory. It is assumed that there is no change to the curvature of the meniscus (i.e. $\theta_0 = \theta_{AT}$) hence the matric suction remains the same. Delage et al. (2008) have evaluated how the if the difficulties arising in the experimental technique of axis translation such as air diffusion, evaporation and condensation effects and air pressurisation

are specifically addressed, axis translation is an “efficient and reliable method of controlling suction.”

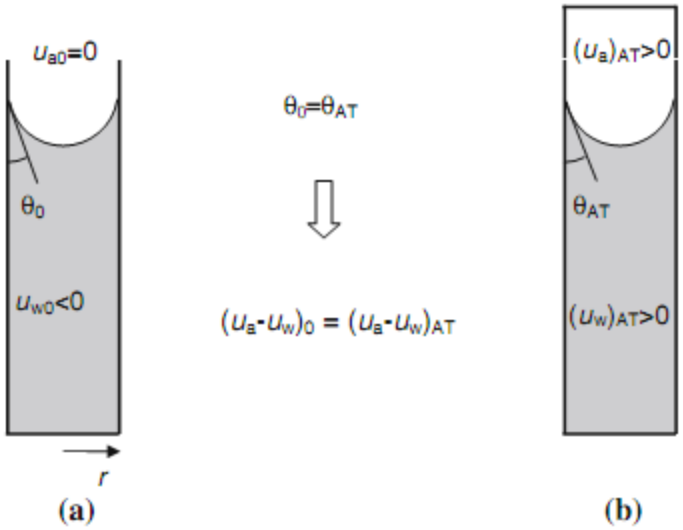

Figure 2.4: Working principle of axis translation technique (Marinho et al., 2006)

3. Chapter 3 – EXPERIMENTAL TECHNIQUES

3.1. Preparation of the sample

The initial soil sample was crushed to pass through a 1.2mm (ASTM #16) sieve; this process was conducted carefully using only rubber mallets and rubber basins to avoid breaking particles and thus affecting the structure of the soil, only to remove aggregate particles from the sample. This was left to air dry at least overnight in the laboratory where it retained a hydroscopic humidity of 1.6%.

3.2. Preparation of sample for testing

When preparing a sample for testing, the required water content was achieved by adding water by spray bottle in measured quantities by weight and mixed thoroughly using spatulas. The determination of the water content was achived using the following equation:

$$M_{s+w} = V * \rho_d * (1 + w)$$

where M_{s+w} is the mass of the soil, V is the total volume of the sample, ρ_d the dry density and *w* the water content, calculated taking into account the hydroscopic humidity.

The sample was then sealed and left to equilibrate over 24 hours to allow the water to fully penetrate the microstructure and an even distribution of moisture throughout the sample. This equilibration time has an important effect on the capillary action within the soil. This can be demonstrated by modelling the structure as shown in Figure 3.1

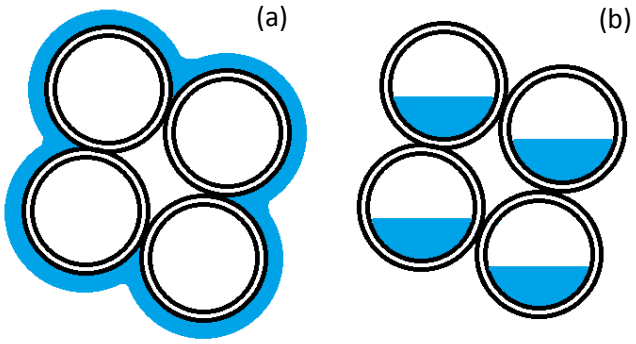

Figure 3.1: Diagram illustrating differences in water distribution in samples (a) immediately after preparation (b) after equilibration overnight

A small part of the prepared sample was then weighed and then dried overnight in the oven to achieve an accurate measurement of actual moisture content. No samples pre- or post-experiment

were handled using bare hands to avoid a distorted reading through absorption of moisture though the skin.

3.3. Compaction of Samples

Proctor (1933) showed that the degree to which a soil can be compacted is dependent on four main factors: the type of soil, the method of compaction, the energy of compaction and the water content of the soil at the time of compaction. To gain a general idea of the compatibility of this soil, both a normal and a modified Proctor curve will be constructed with a static compaction test for comparison. The Proctor test allows for the study of the effect of water content by controlling energy of compaction; the method of compaction and type of soil are clearly also constant. This will also be useful for comparison with previous studies such as that of Barrera (2002) and Buenfil (2007) to identify similarities in behaviour.

In this study we are using four different samples: samples compacted and tested on the dry side, DD; samples compacted on the dry side and wetted before testing, DW; samples compacted on the wet side and dried before testing, WD; and samples compacted and tested on the wet side, WW.

The samples for the suction controlled oedometer, the mercury intrusion porosimetry and the WP4 were compacted in a mould with a diameter of 50mm and a height of 20mm as shown in Figure 3.2.

Figure 3.2: Compaction mould (a) assembled (b) disassembled

3.3.1. Dynamic compaction

3.3.1.1. Standard Proctor Test

The standard Proctor test was carried out according to BS EN 13286-2:2010 with mould size of 100 mm diameter and 120 mm in height; a schematic of the mould is shown in Figure 3.3. The test was carried out using 3 layers with 26 blows per layer. With a rammer of 2.5kg dropped from a height of 300mm. The specific energy of the test can be calculated using the following equation:

$$Specific\ energy = \frac{mass\ of\ rammer * height\ of\ fall * number\ of\ blows\ per\ layer * number\ of\ layers * gravity}{volume\ of\ mould}$$

Which comes to 0.573 MJ/m^3 in the standard proctor.

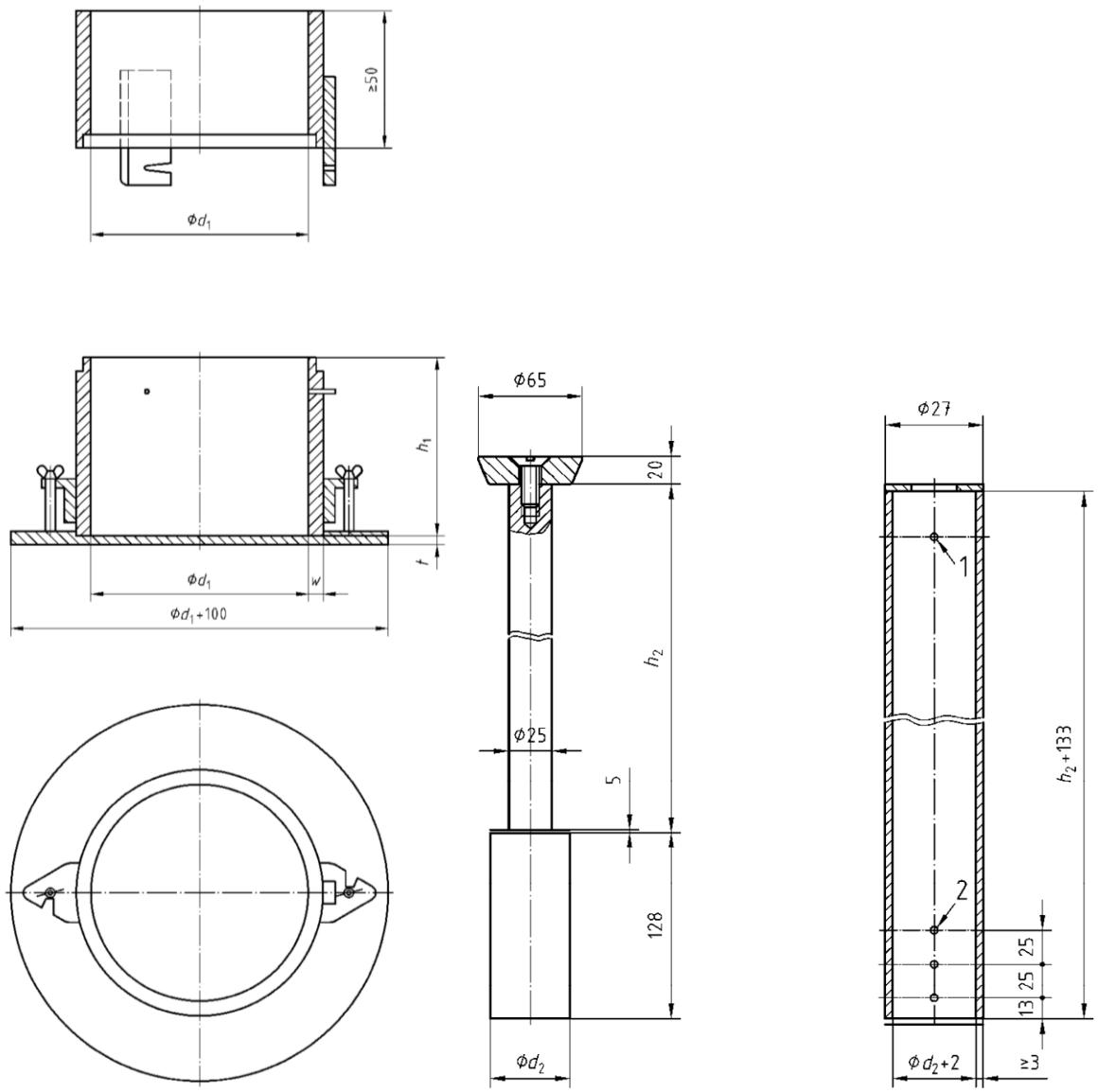

Figure 3.3: Equipment for the Proctor Test (a) the mould and (b) the rammer (from BS EN 13286-2:2010)

3.3.1.2. Modified Proctor Test

The modified Proctor test was also carried out according to BS EN 13286-2:2010 with mould size of 150 mm diameter and 125 mm in height. The test was carried out using 5 layers with 60 blows per layer. With a rammer of 4.5kg dropped from a height of 457mm. The specific energy of the test can be calculated using the same equation as mentioned earlier:

$$Specific\ energy = \frac{mass\ of\ rammer * height\ of\ fall * number\ of\ blows\ per\ layer * number\ of\ layers * gravity}{volume\ of\ mould}$$

Which comes to 2.608 MJ/m^3 in the modified proctor.

3.3.2. Static Compaction Equipment

The compaction equipment consists of a metal mould of 50mm diameter with a 20mm height and a steel piston with a head larger than that of the mould to control the compaction with metal to metal contact when the desired dimensions have been reached. The compaction stress was applied using a computer controlled press shown the photo in Figure 3.4.

Figure 3.4: Computer controlled press with data logging equiment

3.4. Equipment Used in the Study

3.4.1. Mercury Intrusion Porosimetry (MIP)

The MIP technique involves the intrusion of mercury into a sample by applying a pressure to allow it to enter empty pores. The non-wetting property of the mercury prevents from entering pores by capillary action (Micromeritics Instrument Corp.) therefore the pressure applied is inversely proportional to the size of the pores, giving data about the pore size and distribution.

Romero and Simms (2008) have identified four key limitations of MIP; two are a result of the structure of the soil itself: that isolated pores are not measured and constricted porosity means larger spaces are not always detected until smaller pores are penetrated, and the other two a result of the limitations of the apparatus used: the capacity of the apparatus means that some smaller pores are not penetrated and the maximum pore size detected is dependent on minimum practical pressure of the apparatus.

The tests were performed on a mercury porosimeter manufactured by Micromeritics Instruments, AutoPore IV model 9500 which has 2 low pressure chambers and 1 high pressure chamber. The low pressure is applied in a range between 0 and 345kPa and the second, a high-pressure phase in which values are applied in a range between atmospheric and 228MPa. In the low pressure range, the machine uses dry nitrogen (dry air) as a fluid to apply pressure on mercury, while the high pressure range uses oil. The machine and the penetrometer are shown in Figure 3.5.

(a) (b)

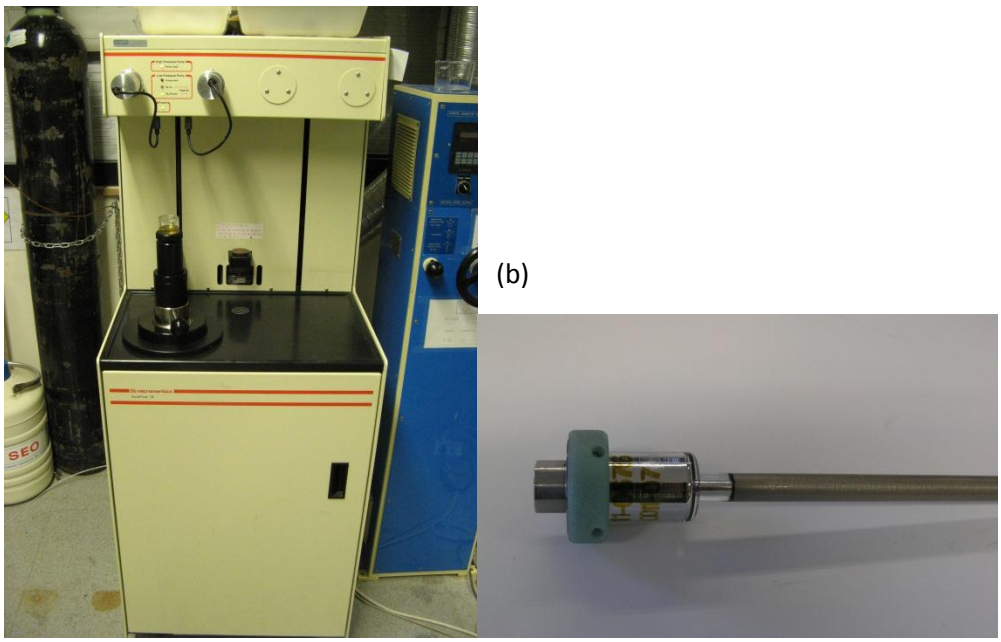

Figure 3.5: (a) Micromeritics AutoPore IV, (b) mercury filled penetrometer

3.4.2. Dew Point Psychrometer

The WP4-T dew point psychrometer, or mirror psychrometer is used in this study, made by Decagon Devices, show in Figure 3.6. This equipment can measure a range of high suctions (above 1.5MPa), with capacity for measuring total suction with a working range of between 1 and 100MPa.

The WP4 operates using the chilled-mirror dewpoint technique. This involves finding the potential of the water within the samples by equilibrating the potential of the water in the air of the chamber

with that of the water in the sample as shown in Figure 3.7. The chamber contains a mirror and photocell that detects condensation on the mirror (Leong et al., 2003) by sending a beam of light towards the mirror and registering any change in the reflected beam (Gómez, 2009). The chamber is sealed and the temperature of the sample is controlled with an infrared thermometer and the temperature of air in the chamber with a thermoelectric (Peltier) cooler on the mirror (Leong et al., 2003). When condensation first appears on the mirror, the water pressure in the air is just sufficient to saturate it, this is the dew-point. At this point the WP4 measure mirror and sample temperature to an accuracy of 0.0001°C (Decagon Devices, 2011).

Equipment calibration was performed daily with salt solutions of sodium chloride (NaCl) with a known concentration (and hence suction).

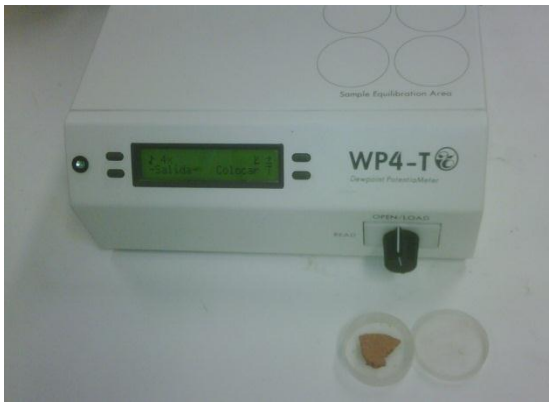

Figure 3.6: WP4-T Dew Point Psychrometer and sample

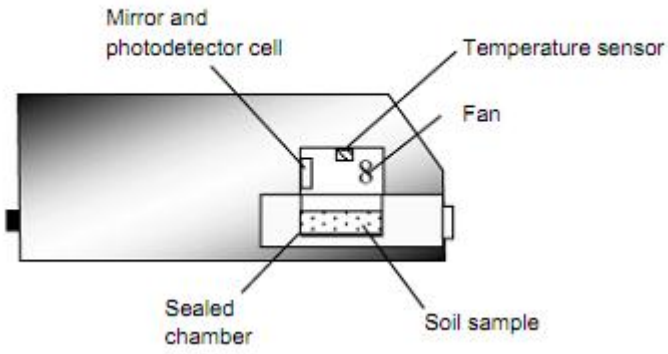

Figure 3.7: Schematic of chilled mirror dewpoint device (Leong et al., 2003)

3.4.3. Suction Controlled Oedometer

The equipment used in the study was developed by the Geotechnical Laboratory at UPC. The sample size is 50mm in diameter with a height of 20mm. Figure 3.8 shows the schematic of the equipment while Figure 3.9 shows photos of the equipment in dismantled into its components and assembled.

The oedometer is split into 3 sections: the base, the central body and the upper section. Within the central body there is the ring containing the sample and connections to control the confining pressure. In between the central body and the upper section, a rubber membrane on which pressure is applied to which is attached a piston of metal and porous stone that controls the transfer of the pressure to the sample. Within the base, a permeable set of metal rings allows water to enter the sample in a controlled manner. There is a rigid frame that surrounds the equipment that supports the micrometer for measurement of deformation.

The measurement and control of air and water to the system was achieved by using volume and pressure digital controlled made by GDS Instruments that has pressure control with a resolution of 1 kPa and volume control with a resolution of 0.5 mm^3/step, shown in Figure 3.10.

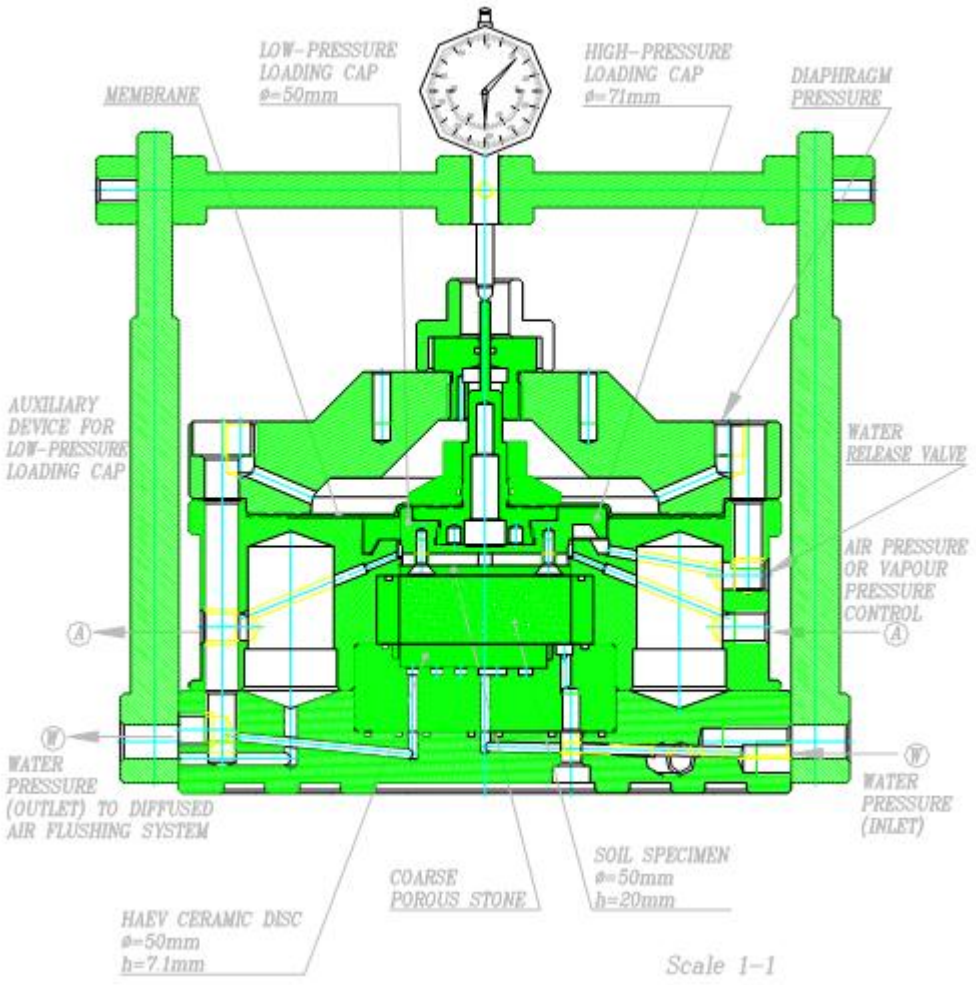

Figure 3.8: Schematic of the UPC Suction Controlled Oedometer (UPC)

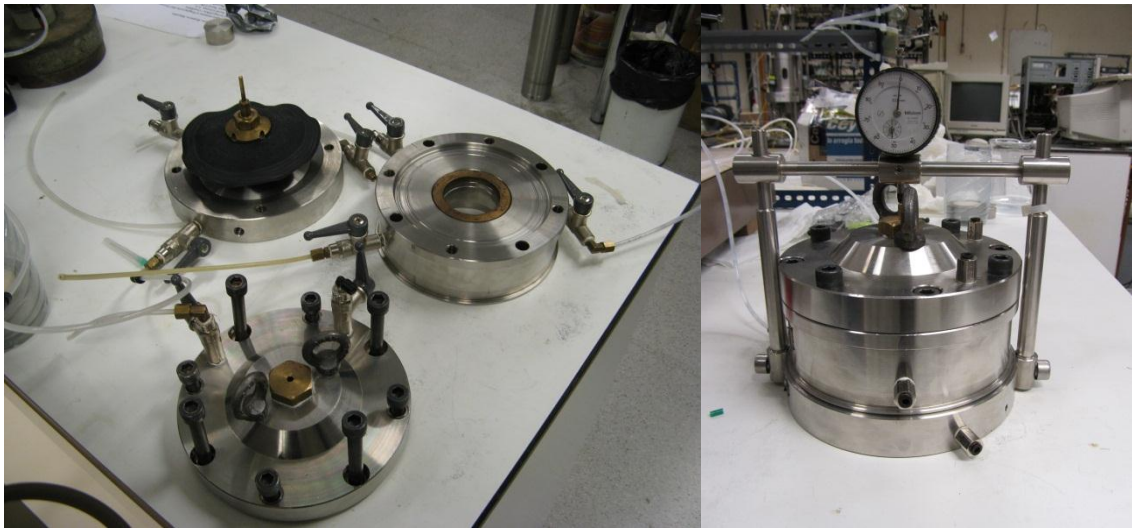

Figure 3.9: Suction Controlled Oedometer in (a) its component parts and (b) fully assembled

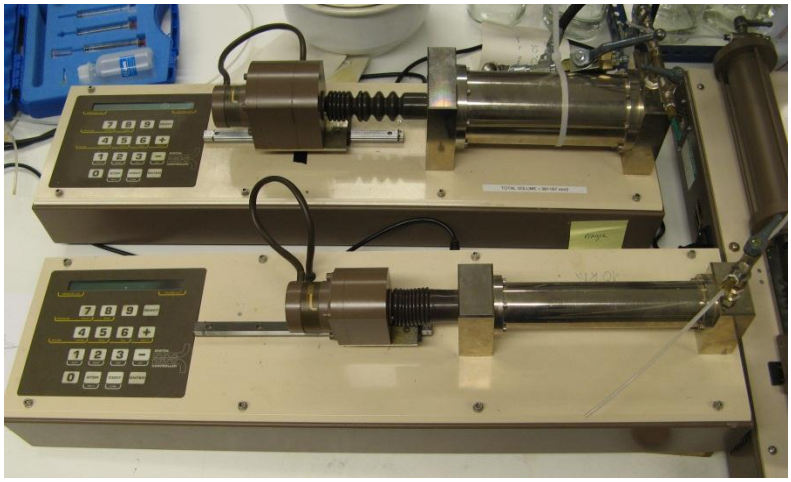

Figure 3.10: GDS volume and pressure controllers

3.4.4. Resonant Column

The resonant column test was developed in studies by Richart (1970), Drnevich (1978) and Anderson and Stokoe (1978). This study uses a “fixed-free” apparatus as first shown in studies by Hall and Richart (1963). The resonant column can be used to find the elastic modulus in small shear deformations, its applicability in relation to other in-situ and laboratory test is shown in Figure 3.11.

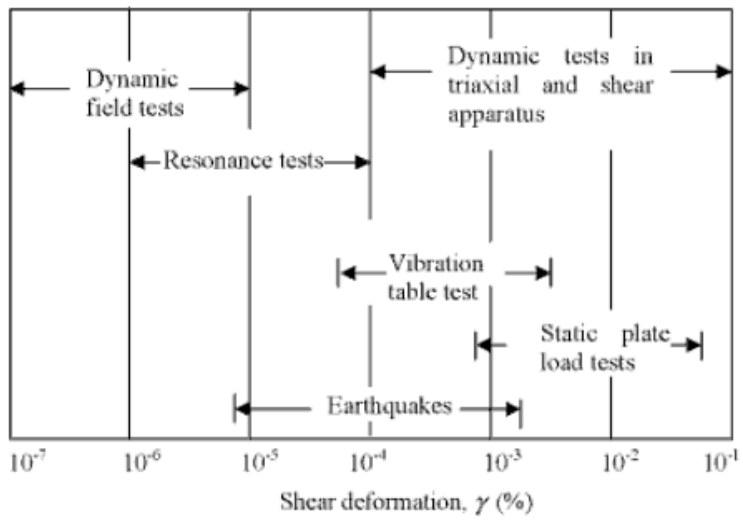

Figure 3.11: Range and applicability of dynamic laboratory tests (Das and Ramana, 1993)

The functionality is based on the transmission of shear waves across the sample. Knowing the velocity of the shear waves, v_s and the density of the material, ρ, the elastic modulus, G can be calculated using the following formula:

$$v_s = \sqrt{G/\rho}$$

In a cylindrical sample that is fixed at one end with cyclical shear being applied at the other, a resonant frequency can be determined by the geometry of the sample and the transmission velocity.

For a given sample height, the resonant frequency depends on a rigidity modulus and for an elastic material set up as shown in Figure 3.12, dynamic equilibrium is given by the following expression (Das and Ramana, 1993)

$$2\pi f_r L\sqrt{G/\rho} \cdot \tan 2\pi f_r L\sqrt{G/\rho} = \frac{J_s}{J_m}$$

Where:

f_r= the resonant frequency

L = the height of the sample (in this study 76mm)

J_s = mass polar moment of inertia of the soil sample

J_m = mass polar moment of inertia of the attachments with mass, m.

This equation is of the form $\alpha \tan \alpha$ which has a numerical solution of the form:

$$G = K \cdot {f_r}^2$$

Where K is function of J_s, J_m, L, ρ. In this study the value of K is calculated as 0.03786 if the frequency is measured in Hertz and G in MPa.

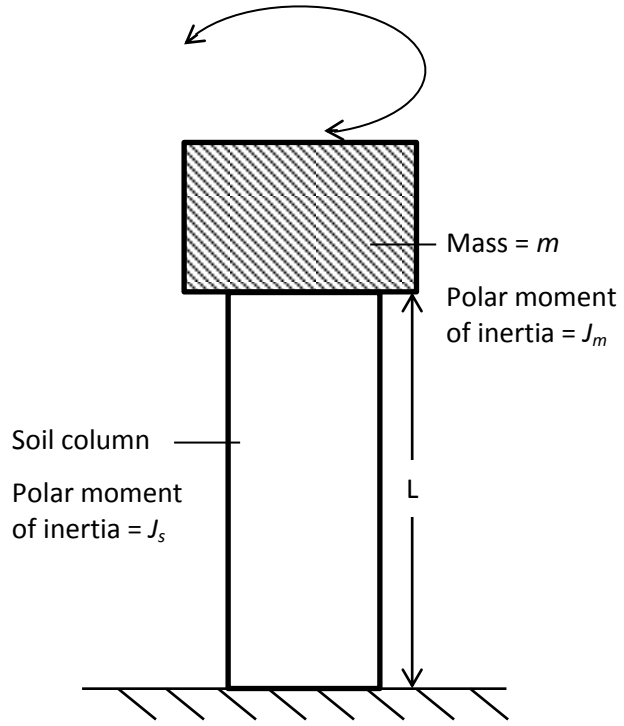

Figure 3.12: Schematic of the apparatus (adapted from Das and Ramana, 1993)

The application of cyclical shear at the upper extremity of the sample whilst it is fixed at the base results in an angular shear deformation as shown in Figure 3.13.This value is measured by an accelerometer, with the angular deformation at the top calculated through the double integration of the acceleration.

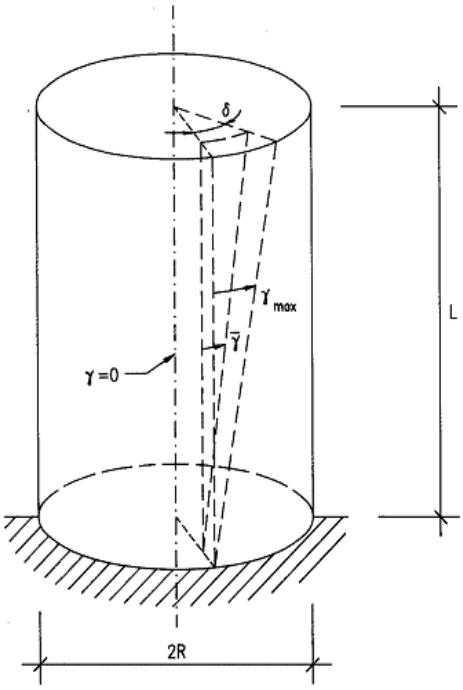

Figure 3.13: Geometric description of angluar deformation (Suriol, 1993)

To calculate a value of mean angular deformation, $\bar{\gamma}$, the following calculation is employed (Suriol, 1993):

Hence, the maximum angular deformation would be:

$$\gamma_{max} = \frac{R \cdot \delta}{L}$$

From geometry and substitution:

$$\bar{\gamma} = \frac{2}{3}\gamma_{max} = \frac{2}{3} \cdot \frac{R \cdot \delta}{L}$$

Substitution for δ gives:

$$\bar{\gamma} = K_2 \cdot \frac{V_e}{{f_r}^2} \cdot \frac{2R}{3L}$$

Where V_e is the effective output voltage from the accelerometer. The value of the constant, K_2, is obtained by finding the stress-acceleration relationship of a known calibration sample (in this case of aluminium). In this study, a value of K_2 of 97.8 is used.

Figure 3.14 shows a schematic of the resonant column equipment whilst Figure 3.15 shows a photo of the accessories to the equipment.

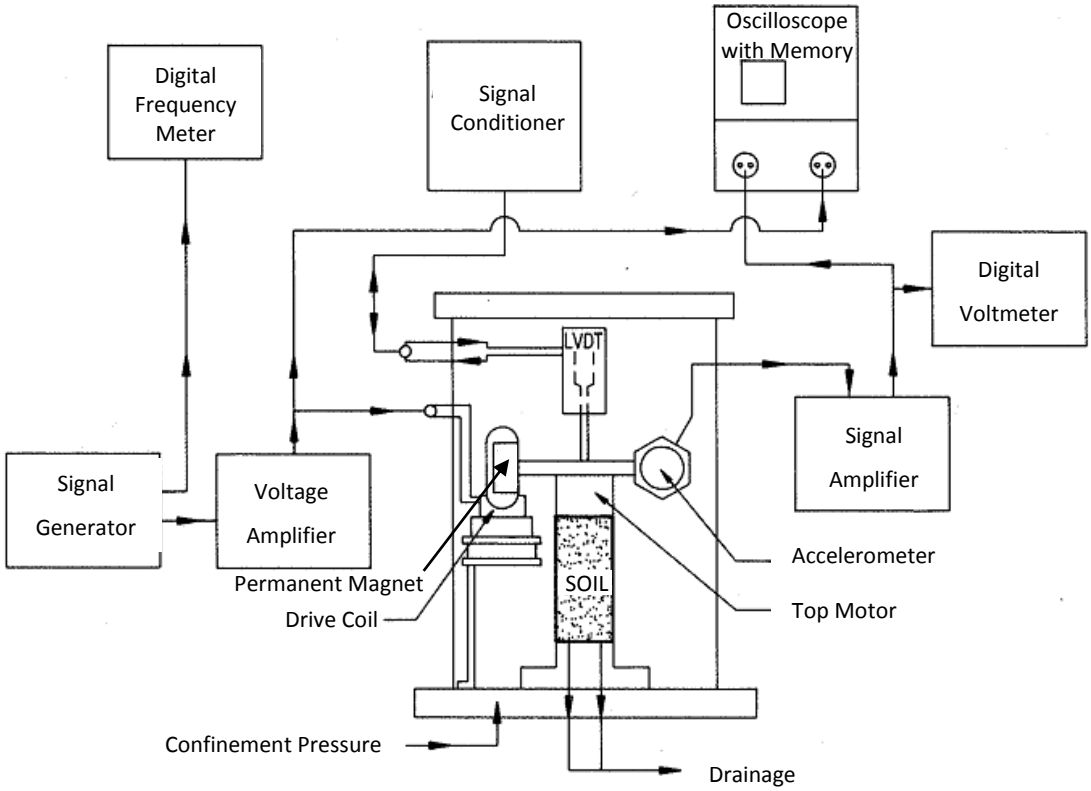

Figure 3.14: Schematic of Resonant Column (adapted from www.civil.ubc.ca and Suriol, 1993)

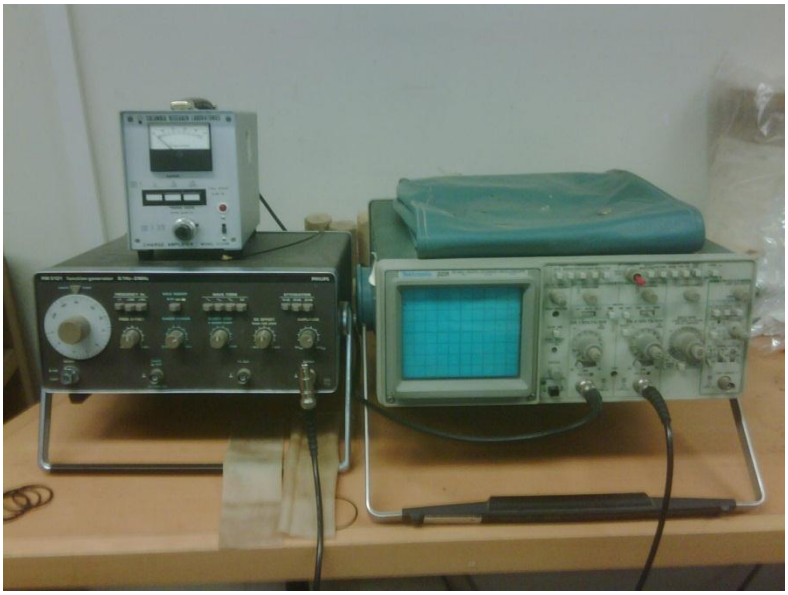

Figure 3.15: Accessories to the resonant column equipment including the oscilloscope

3.5. Experimental Procedure

3.5.1. Classification

3.5.1.1. Separation through sieving

A sample was sieved though 4 sieve sizes: 1.18, 0.425, 0.15 and 0.075mm (#16, 40, 100 and 200 respectively in ATSM numbering). The procedure was carried out according to UNE 103-101/95.

3.5.1.2. Sedimentation

For particles sizes smaller than 0.075mm, a process of sedimentation was used according to UNE 103-102/95. By leaving a solution of the soil with distilled water and sodium polyphosphate and sampled at predetermined time intervals as shown in Table 3.1:

Table 3.1: Sedimentation times

Particle Size	Sedimentation Time
0.04	00:01:00
0.02	00:04:02
0.005	01:04:27
0.002	06:42:48

3.5.1.3. Normal and Modified Proctor Tests

The normal Proctor curve was constructed using six points of water content. The soil was prepared to the required water content the day prior to testing and covered overnight. The same soil sample was reused for each test. Four different water contents were used to construct the modified Proctor curve.

3.5.1.4. Static Compaction

The samples were compacted slowly at rate of 1mm/min and then left to equilibrate for 10 minutes before being removed from the press and removed from the mould. The results can be seen in Figure 3.16, showing a compaction stress of 185-190kPa.

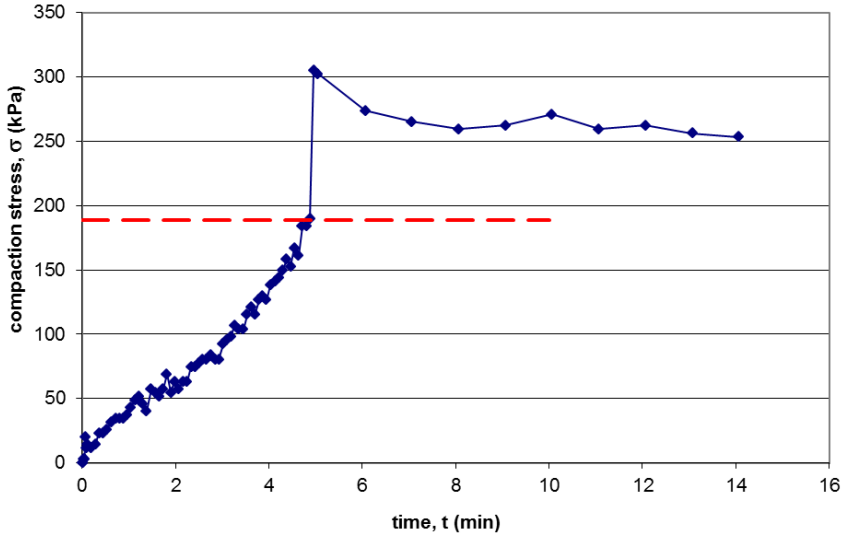

Figure 3.16: Static compaction data from sample compacted at a water content of 12.5%

3.5.2. Porosimetry: MIP

The tested samples were compacted using static compaction then cut into cubes with dimensions of about 1cm^3. They were then freeze dried, a process that quickly freezes the water in the pores using liquid nitrogen leaving the microstructure of the sample intact and removing tension caused by air-water interfaces from the surface of the pores.

The samples were placed inside the penetrometer and weighed. The penetrometer is placed into the low pressure port of the MIP equipment where the air is removed by vacuum then filled with mercury under incrementally rising pressures to fill the larger pores of the sample. The penetrometer is then removed and transferred to the high pressure port where the mercury continues to be forced under pressure to fill the smaller pores in the sample.

After the filling stage, the pressure is decreased in a controlled manner to remove the mercury. The volume of mercury intruded is often much larger than that removed due to hysteresis that occurs during the filling stages.

3.5.3. Retention Curve

To obtain the curve showing the relationship between suction and water content, two methods have been employed during this study: MIP and the WP4 psychrometer. There are factors that directly influence the shape of the retention curves such as particle size, mineral composition and soil structure. For small values of suction (highly saturated samples) the structure of the soil is the most influential factor, i.e. capillary action and pore size and distribution whereas for high values of

suction the surface area of the fine particles is the most important as the water is almost all to be found absorbed into the soil particles.

3.5.3.1. Dew-Point Potentiameter

For values of suction above 1.5 MPa, measurements were conducted using the WP4-T dewpoint potentiometer. Before the first measurement of the day, the equipment must be calibrated using a salt solution of known concentration. This ensures the accuracy of the measurement, especially in the low suction range (between approximately 1 and 4 MPa).

The sample is compacted using static compaction and the cut down to fit in the specifically sized container. The container and sample are weighed together then placed in the drawer which when closed, seals the sample in the measuring chamber. Turning the dial to the read position starts the temperature equilibration within the chamber and a beep and a flashing light indicate that the measurement has been achieved.

The reading is taken twice to gain an accurate reading then the sample is reweighed then allowed lose approximately 0.02g of moisture by evaporation in air. The sample is sealed and left to equilibrate for 24 hours.

3.5.3.2. MIP

To measure the lower ranges of suction, the intrusion of mercury using the MIP was used. To determine the retention curve from MIP data, the hydraulic parameters of the soil are required for retroanalysis. The methodology of this is described by Romero (1999):

The water content is calculated:

$$w = \frac{e}{G_s} Sr$$

Where Sr, the degree of saturation, can be calculated using the volume of pore not intruded by mercury:

$$Sr = 1 - Sr_{nw}$$

Where Sr_{nw} is the non-wetted degree of saturation:

$$Sr_{nw} = \frac{e_{nw}}{e_o}$$

Combining these, we arrive at:

$$w = \frac{e}{G_s} Sr = w_{sat}(1 - Sr_{nw})$$

Using the Washburn Equation:

$$p = -\frac{4\sigma_{Hg} \cos \theta_{nw}}{d}$$

And given that suction can be shown to be:

$$s = \frac{4\sigma \cos \theta_{nw}}{d}$$

We can related suction and intrusion pressure, p such that:

$$s \approx 0.196p$$

3.5.4. Suction Controlled Oedometer

The suction controlled oedometer determines the compressibility of the soil along loading-unloading paths (change in net vertical stress) and wetting-drying (suction change) under oedometer conditions (no lateral movement).

The study consisted of three tests, two with samples of DD, one at 20kPa and one at 400kPa and a third with a WD sample for comparison at 400kPa. The samples were statically compacted with a dry density of 1.68 g/cm^3 and the water content of 12.5% (±0.3%) for the dry samples and 17.5% for the wet samples.

The initial set up of the sample involved the application of suction of 100kPa then the samples were loaded at rate of 146 s/kPa then allowed to equilibrate overnight. The unloading was then conducted at a rate of 72s/kPa. The tests were conducted under undrained conditions.

3.5.5. Resonant Column

3.5.5.1. Preparation of samples

The sample was statically compacted in the mould shown in Figure 3.18 which has a diameter of 38mm and a height of 76mm. It should be noted that the compaction energy of the samples of 12.5% was considerably higher than those of 17.5% water content.

To achieve the wetting-drying paths as shown in Figure 3.17, the following methods were employed. To achieve a wet to dry path, the sample was compacted at 17.5% then left to dry in a humidity-controlled environment over a period of 6 days until it achieved the required water content. The sample was then measured to ensure that there was no volume change during the drying process, i.e. constant dry density. To achieve the dry to wet path, the sample was compacted but left in the mould and placed, on top of a porous stone and filter paper, into a basin of water and left to absorb water until saturated. The piston was left above the mould with a small weight upon it to prevent swelling during saturation.

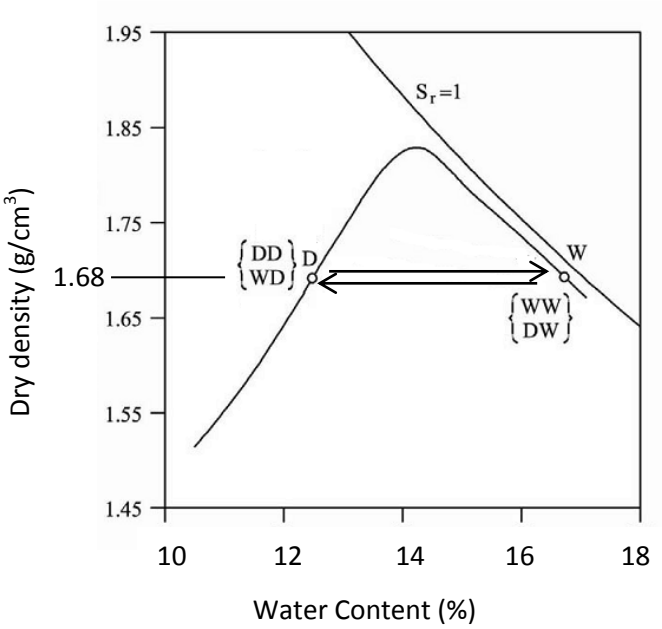

Figure 3.17: Wetting and drying paths of sample

Figure 3.18: Mould used in the compaction of samples for the resonant column test

3.5.5.2. Preparation of equipment

The sample was mounted together with a metal plug for the transference of the shear stress into the equipment using a rubber membrane and 4 rubber O-rings as shown in the photos in Figure 3.19.

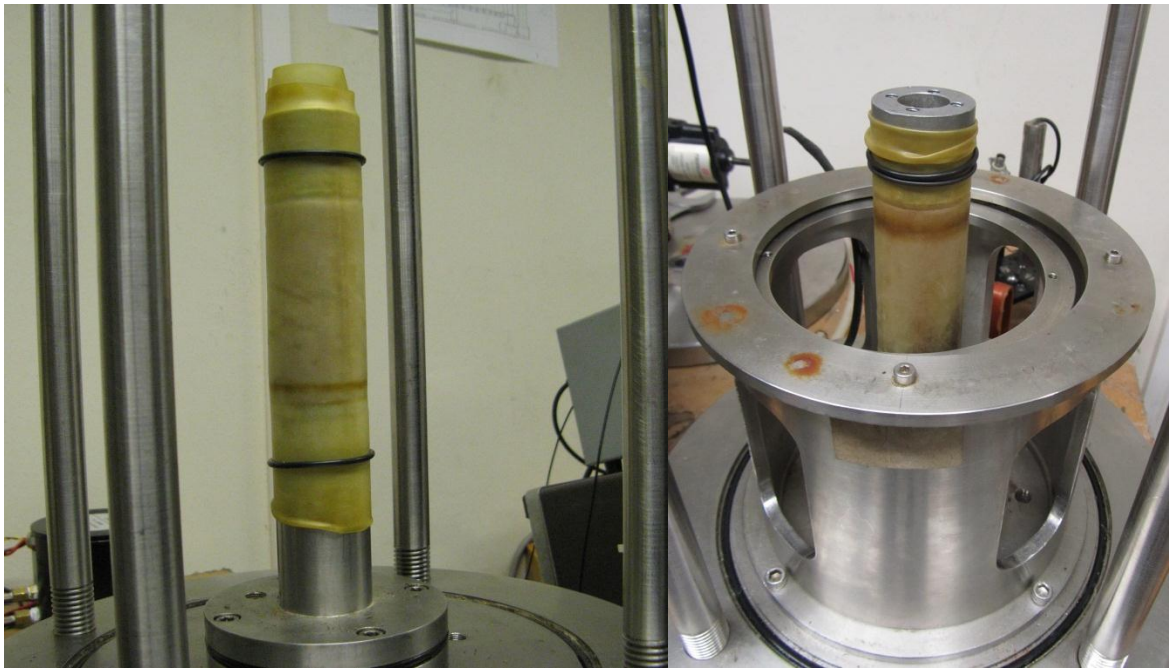

Figure 3.19: Photos showing sample mounted in resonant column equipment

The apparatus onto which the magnets and coils were mounted, was attached via screws to the metal plug as shown in Figure 3.20 with careful attention paid to ensuring that the magnets and the coils were not in contact at any point on the equipment.

Figure 3.20: Photo showing the copper coils and magnets of the top cap of resonant column

The containing cylinder is then placed over the entire system and sealed with the top lid onto which is mounted the pressure gauge as shown in Figure 3.21.

Figure 3.21: Photo showing resonant column fully assembled.

The confinement pressure was then set to 80kPa; preliminary tests were set at 300 kPa but this caused compression and deformation of the sample causing a large change in dry density.

3.5.5.3. Obtainment of Results

The system of magnets and coils applies a shear stress to the sample and the voltage as measured by the accelerometer is displayed on the oscilloscope. The resonant frequency is obtained by varying the oscillation frequency until the response (in terms of the angular deformation of the soil) is in phase with the excitation (in terms of torque). Viscous behaviour considered by measuring the rate damping.

4. Chapter 4 – RESULTS AND INTERPRETATION

4.1. Classification

Table 4.1 shows the results of the granulometry. We can see from Figure 4.1 that the soil is fairly well graded with a small jump between #40 and #100. Over 50% of the material passes through #200 so we can call this fine material, although there is a majority of material classified as sand as can be seen from Table 4.2.

The Attemberg limits were calculated according to ASTM-D4318, with the material passed through sieve #40. In Casagrande's Unified Soil Classification System (USCS), we can see from Table 4.2 that as the soil has a plasticity index just above 7, we technically classify the soil, called here CN – VS as a low plasticity clay, CL however as can be seen from Figure 4.2 its proximity to low plasticity silt region suggests that the behaviour of the soil will be more typical of a low plasticity silt, ML.

Table 4.1: Fraction of particles passing in granulometry

ASTM Standard	Sieve Size	Percentage Passing
#16	1.18	100
#40	0.425	88.93
#100	0.150	58.66
#200	0.075	53.05
Sedimentation	0.04	44.05
	0.02	34.05
	0.005	22.80
	0.002	16.66

Table 4.2: Soil characteristics

Definition	Laboratory Results
Sand	46.95%
Silt	36.39%
Clay	16.66%
Attemberg Limits	
Liquid Limit	21.06
Plastic Limit	13.71
Plasticity Index	7.35

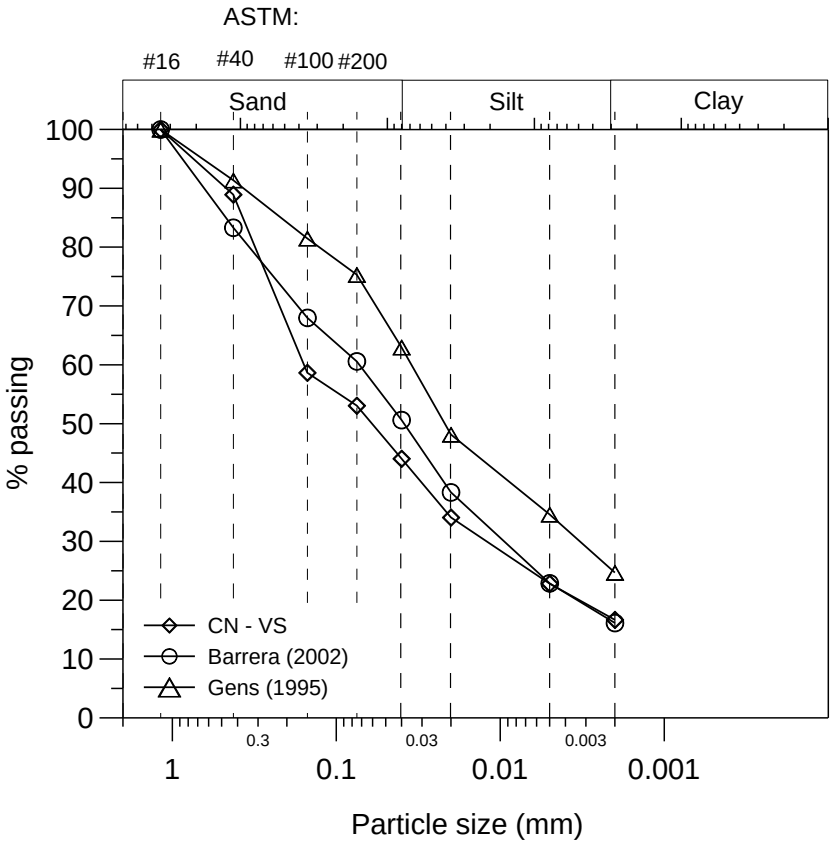

Figure 4.1: Granulometric Curve

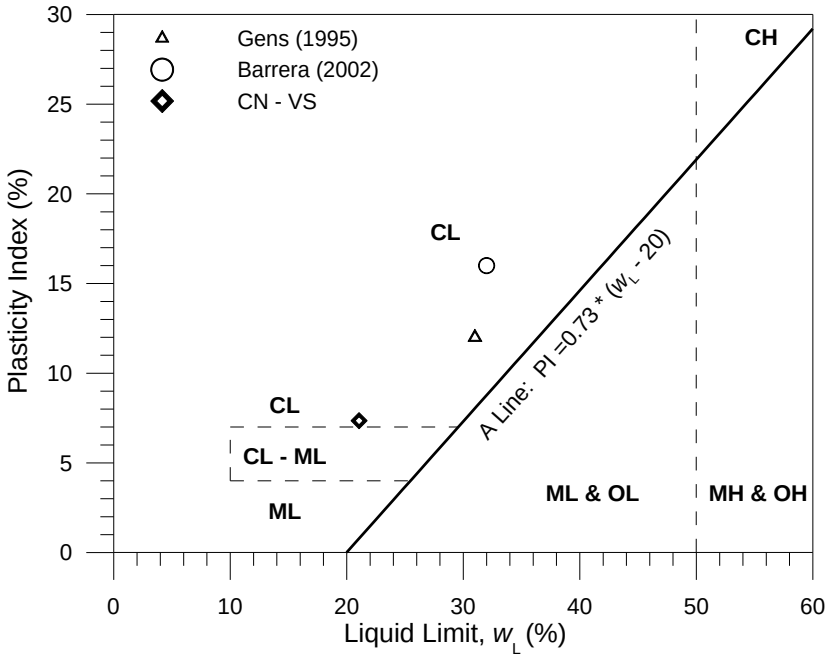

Figure 4.2: Soil Plasticity Chart

4.2. Proctor Tests

Comparison of the normal Proctor curves with those of Buenfil show that this sample is much more compressible and able to compact to much higher dry densities for a given compaction energy.

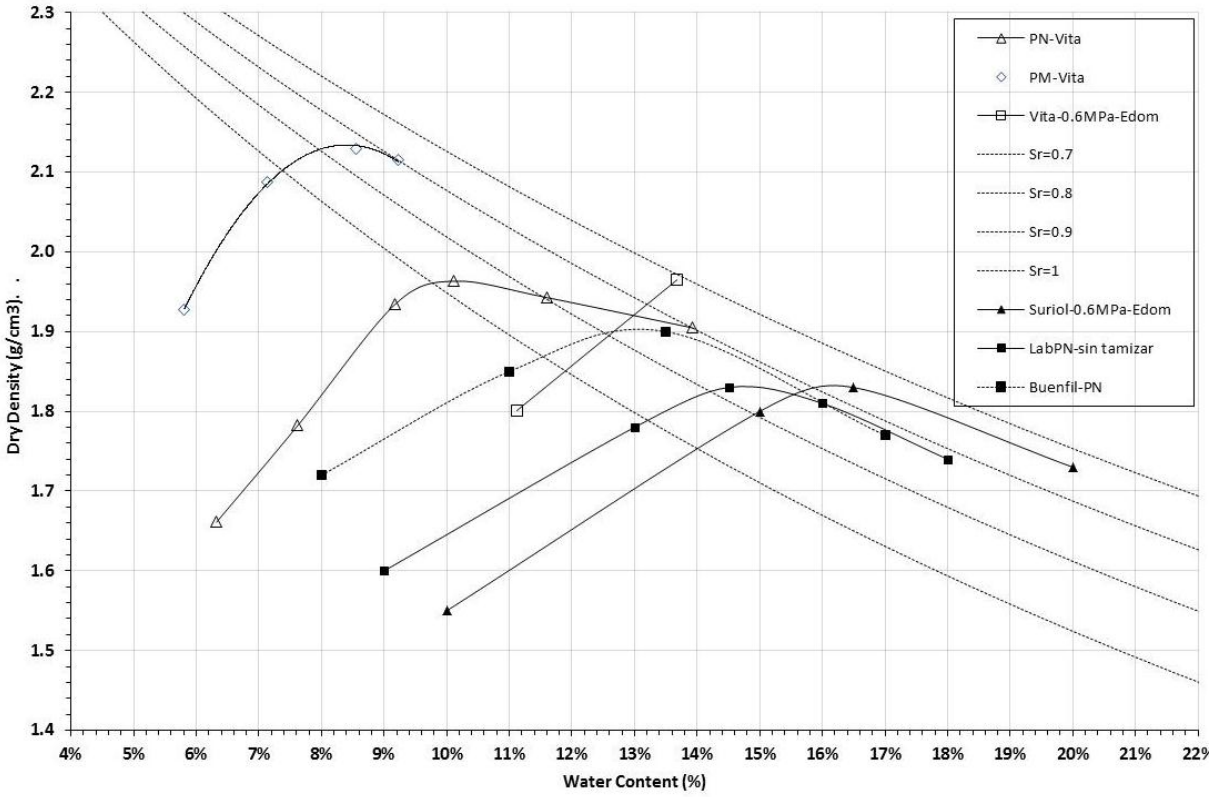

Figure 4.3: Results of Protor Tests compared with previous data

$(\gamma_d)_{opt}$	Optimum Humidity
Normal Proctor	9.6%
Modified Proctor	8.5%

Alonso (2007) describes typical values of the ratio between modified Proctor optimums and normal proctor optimum as 0.952 for an ML soil, however in this case we can see that

$$\frac{(\gamma_d)\text{opt} - \text{NP}}{(\gamma_d)\text{opt} - \text{MP}} = \frac{0.085}{0.096} = 0.885 \ < 0.952$$

This shows this soil responds more to dynamic compaction that is normal for an ML soil, perhaps indicating higher compressibility.

4.3. Mercury Intrusion Porosimetry

Table 4.3: Sample data from MIP tests

Sample	$w_{compaction}$	w_0	e_0	e_{MIP}	Percentage Intruded
DD	12.2%	12.2%	0.586	0.539	92.0%
DW	12.4%	18.0%	0.595	0.502	84.4%
WD	17.4%	11.1%	0.595	0.466	70.6%
WW	17.1%	17.1%	0.595	0.42	78.3%

4.4. Intrusion-Extrusion Curves

Figure 4.4 shows the results of the MIP intrusion-extrusion process, we can see that the value of e_0 and e_{MIP} are different shown by the differences between the measured e and the maximum e intruded. The lower value of e_{MIP} can be attributed to the apparatus not have the capacity to enter the smallest pores (Romero and Simms, 2008) or to a lesser extent, the difference between the amount of water removed through sublimation (as achieved through freeze-drying as conducted with the samples for the MIP testing) and through oven drying, the manner in which e_0 was initially calculated (Tarantino and Simms, 2008). These differences are shown by giving a percentage intruded as shown in Table 4.3.

The results of MIP intrusion-extrusion can be used to evaluate the ratio between e_{micro} and e_{macro}. Delage and Lefebre (1984) proposed that a sample could be broken down into inter-aggregate (constrained) porosity and intra-aggregate (reversible) as shown in Figure 4.5 and that these two porosities can be obtained from intrusion-extrusion data as shown. Their proposal was that the extrudable and unintrudable porosities combined reflect the value of the intra-aggregate (reversible) porosity and assumed that the larger inter-aggregate pore space corresponds to the entrapped porosity.

These results show that sample compacted on the wet side of optimum show a slightly higher $e_{inter-agg}$ than those compacted on the dry side but the results are not definitive, given the similarity in the $e_{inter-agg}$ between the DW and WW samples. We can also see from Table 4.4 that the limit of macro and micro is much higher in those samples compacted on the dry side, giving a delimiting zone of 56-61 for the samples compacted on the wet side and 86 to 156 for samples compacted on the dry side as shown in Figure 4.7.

Suriol and Lloret (2007) define the microporosity and macroporosity as shown in Figure 4.6. Table 4.4 shows the values of e_{micro} and e_{macro} as calculated using this methodology in comparison with that

of Delage and Lefebre. These results show much more clearly the trend towards greater e_{micro} for samples compacted on the wet side.

Table 4.4: Microstructural porosity data

Sample	e_0	$e_{intra-ag}$(D&L)*	$e_{inter-ag}$ (D&L)*	Macro-Micro Limit (nm)	e_{macro} (S&L)*	e_{micro} (S&L)*
DD	0.586	0.506	0.08	86	0.3	0.286
DW	0.595	0.45	0.145	156	0.3	0.295
WD	0.595	0.387	0.208	61	0.219	0.376
WW	0.595	0.437	0.158	56	0.19	0.405

*(D&L refers to Delage and Lefebre (1984); S&L refers to Suriol and Lloret (2007)

A more useful method of comparison might be to use this data to calculate a ratio, ξ_m, between e_0 and e_m (Alonso, 2011) as calculated in Table 4.5. Figure 4.8 shows there is strong correlation between the water content at compaction and ξ_m rather than between water content at testing and ξ_m. Again, the transmission of information that controls behaviour arises from the water content at compaction and e_{micro} seems little affected by wetting and drying cycles.

Table 4.5: Microstructural ratios

Sample	ξ_m (D&L)*	ξ_m (S&L)*
DD	0.08	0.3
DW	0.145	0.3
WD	0.208	0.219
WW	0.158	0.19

*(D&L refers to Delage and Lefebre (1984); S&L refers to Suriol and Lloret (2007)

When looking at the intrusion-extrusion curves, we can see again the similarities between the DD and DW samples and the WW and WD samples as shown in Figure 4.7. The drying of the wet sample causes a shift down, with a lower non-intruded porosity, the same occurred in the wetting of the dry sample. The latter is consistent with the findings of Suriol and Lloret (2007) but the shift down from DD to DW is not. The main explanation for this could be in the control of the wetting and drying, with the samples from this study, the volume was controlled not the suction as was the case in the study of Suriol and Lloret (2007).

When looking at the extrusion curves, we can see that the slopes for the WD and WW are very similar but those of the DD and DW are quite divergent, with the DW sample showing much steeper slope than the DD indicating a more reversible intruded pore space.

However consistently with the other results, we can see that the behaviour is much more heavily influenced by the water content at compaction.

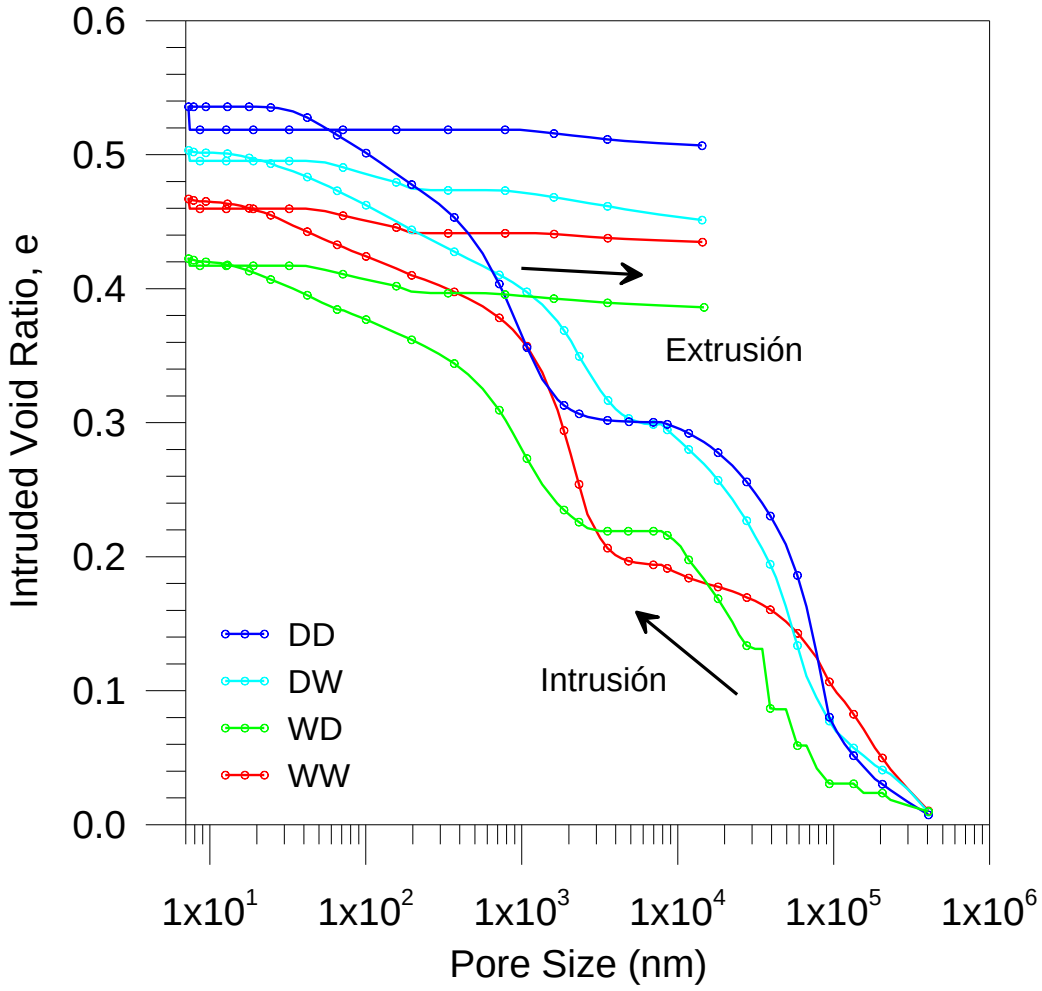

Figure 4.4: Complete intrusion-extrusion data

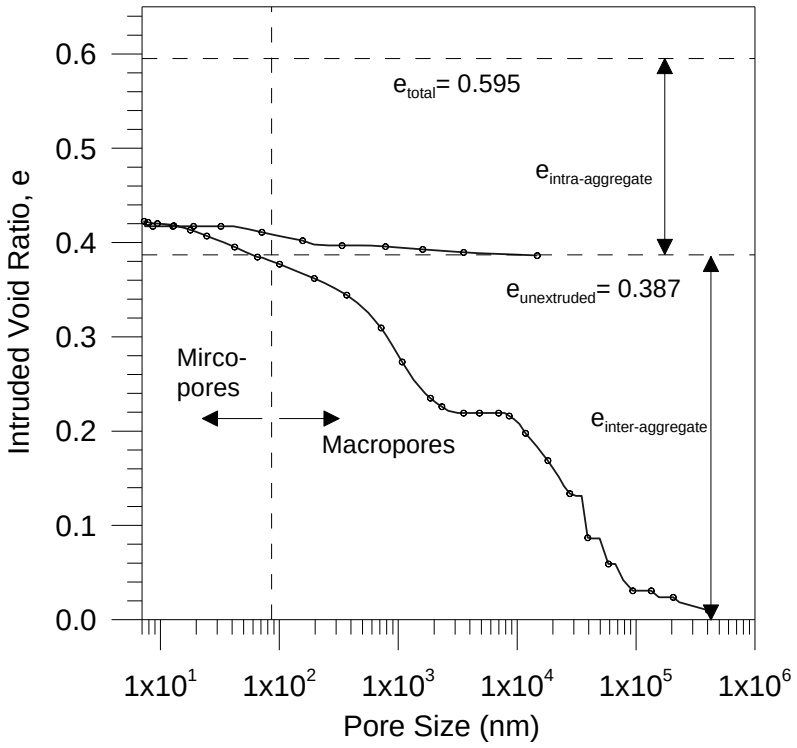

Figure 4.5: Differentiation between inter- and intra- aggregate pore (adapted from Delage and Lefebre, 1984)

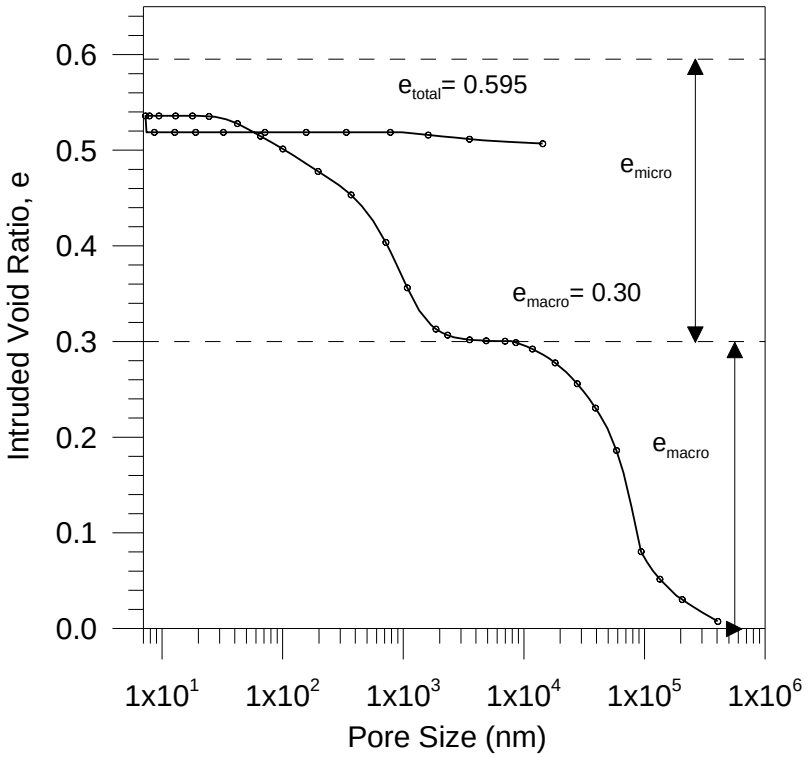

Figure 4.6: Comparision of e_{micro} and e_{macro} (from Suriol and Lloret 2007)

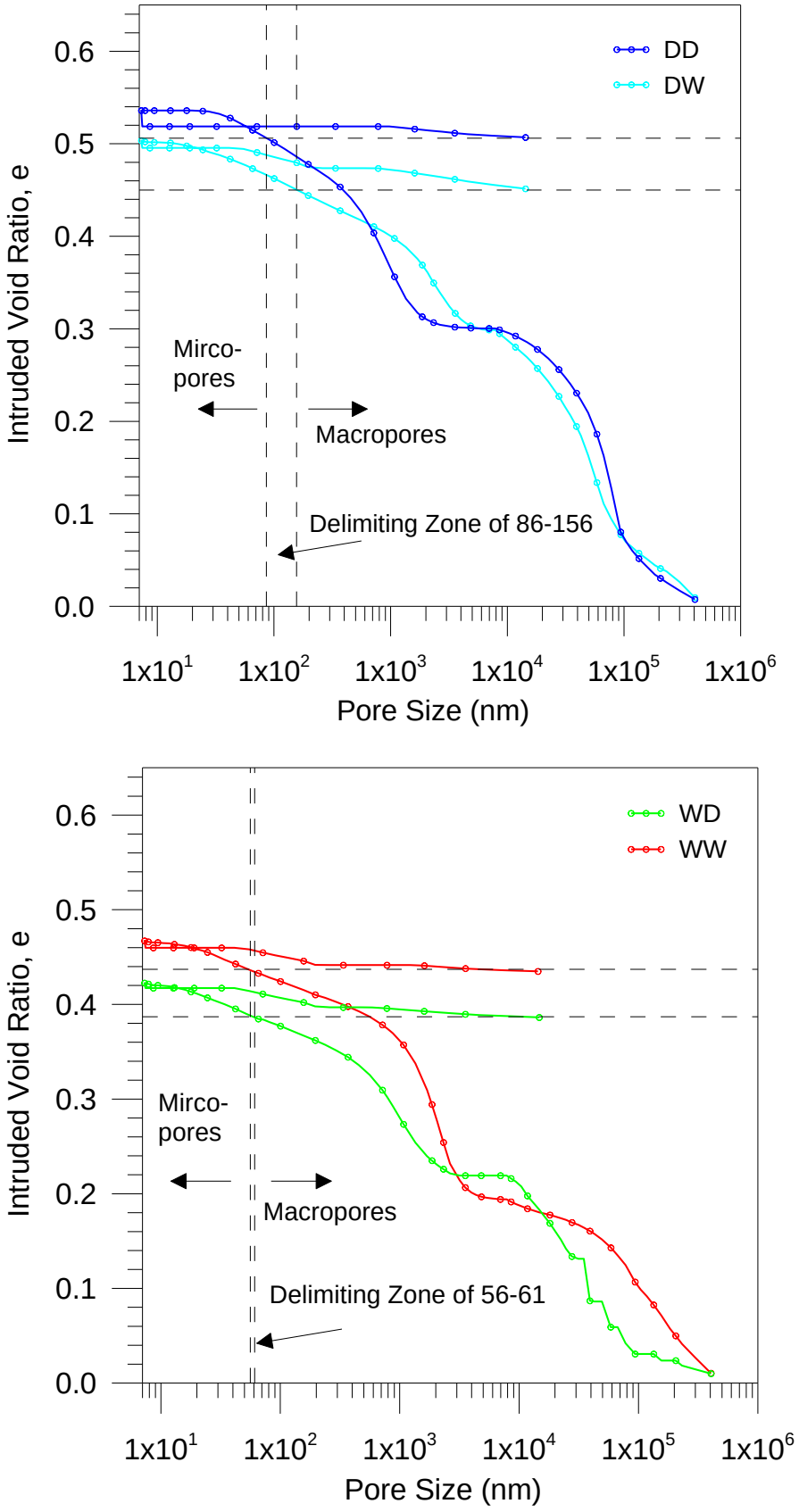

Figure 4.7: Comparision of (a) DD and DW (b) WW and WD

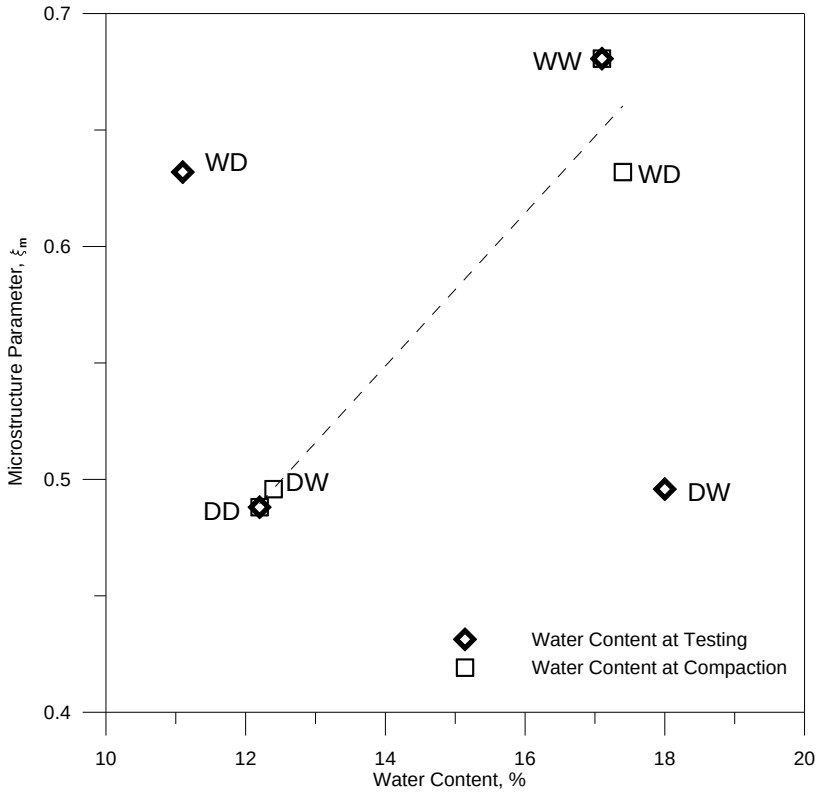

Figure 4.8: Trends in e_{micro} with water content

Pore Size Distribution

Figure 4.9 shows the results from the mercury intrusion porosimetry. We can that for pores smaller than 200nm, the PSD is little affected by either current water content or that at compaction, this indicates that behaviour in this range is controlled other factors such as soil mineralogy and particle size.

The results from the WD sample show a discrepancy in the readings in the macro pore region, where there are a number of anomalous results causing an oscillation between 0 pore size density and very high pore size densities; this is probably caused by machine error in the readings. With the data, we can either disregard the reading entirely or take the envelope that can be seen around the readings as the true result. Figure 4.11(b) shows that we have used an estimation of the true results in the analysis.

We can see if we compare the WW and DD samples as shown in Figure 4.10, that the DD sample has two clear peaks, one in the micro scale at around 800nm and one in the micro scale at around 80000nm whereas the WW sample has one more defined peak in the intermediate range at around 2000nm. This is consistent with the finding of Gens et al. (1995) and Suriol and Lloret (2007) of bimodal and single peak distribution. There is a small peak in the macro range in the WW sample which may be a result of pockets of water that occurred due to the sample being very close to saturation.

When comparing the results of the DD and DW samples as shown in Figure 4.11(a), we can see clearly that shape of the curve is very similar indicated that the pore size distribution is determined by the water content at compaction, not at testing. However, we can see a shift from 800nm to 2000nm for the micro-pore peak, this can be attributed to perhaps a small amount of swelling, but there little effect on the height of the peak. This indicates that there has been no significant change to the micro-porosity. Due to the fact that there was no overall volume change in the sample, we must assume that this was off-set by separate factor, such as a decrease in the number of macro pores. However, it may simply be attributed to slight differences in the construction of the two samples. A significant drop in the macro-pore peak can be observed, indicating that there has been some alteration to the macro-pores during drying.

In Figure 4.11(b) we can see that there is an apparent drop in the macro-pore peak, however due to the discrepancies in the results in this range of the WD sample, this cannot be definitively identified. The micro peaks are very similar; this indicates that the micro-porosity has been affected by the drying process to bring the WD sample in line with the DD sample in this pore range.

In contrast with this, we can see that there are large variations in the pore size distribution between the WW and DW samples as seen in Figure 4.12(a), with the DW sample showing larger densities of macro-pores than the WW sample and a lower peak in the micro region. However, both showed a peak at around 2000nm with similar but not exactly corresponding peaks in the macro range. The development of the macro-porosity shows that this sample has a much greater collapse potential than that of the WW. This has significance when dealing with compacted soil in an engineering context.

We can see the DW has two definitive peaks, with one larger one in the macro range, compared with the WW which has one clear peak in the intermediate-micro region with a small raise in the macro range. This shows that the microstructure at compaction plays a large role in pore size distribution, and the sample has a "memory" for the microstructure created during compaction. This reinforces the theory that the microstructural behaviour of the sample is much more controlled by its water content at compaction rather than at the time of testing.

If we look at the WW and WD in Figure 4.12(b), if we again alter the results to omit the anomalous results and look at the overall pattern, we can see that there has been a slight shift in peaks towards the micro, indicating a small amount of shrinking however commenting on the apparent development of the macro porosity would be unjustified since again we are unclear as to the true distribution in this region, and the alteration shown is only an approximation.

These results indicate that even if there is no overall change in volume of the sample, this does not indicate that there is no change to the microstructure and that some changes in behaviour of the sample can be attributed to restructuring within the sample rather than swelling and shrinking behaviour.

Overall looking at Figure 4.11(b) and Figure 4.12(a) we can comment that the size of the pores where the peaks fall seems to be more controlled by the current humidity of the sample but from Figure 4.11(a) and Figure 4.12(b) the distribution of the porosity is more affected by the humidity at compaction.

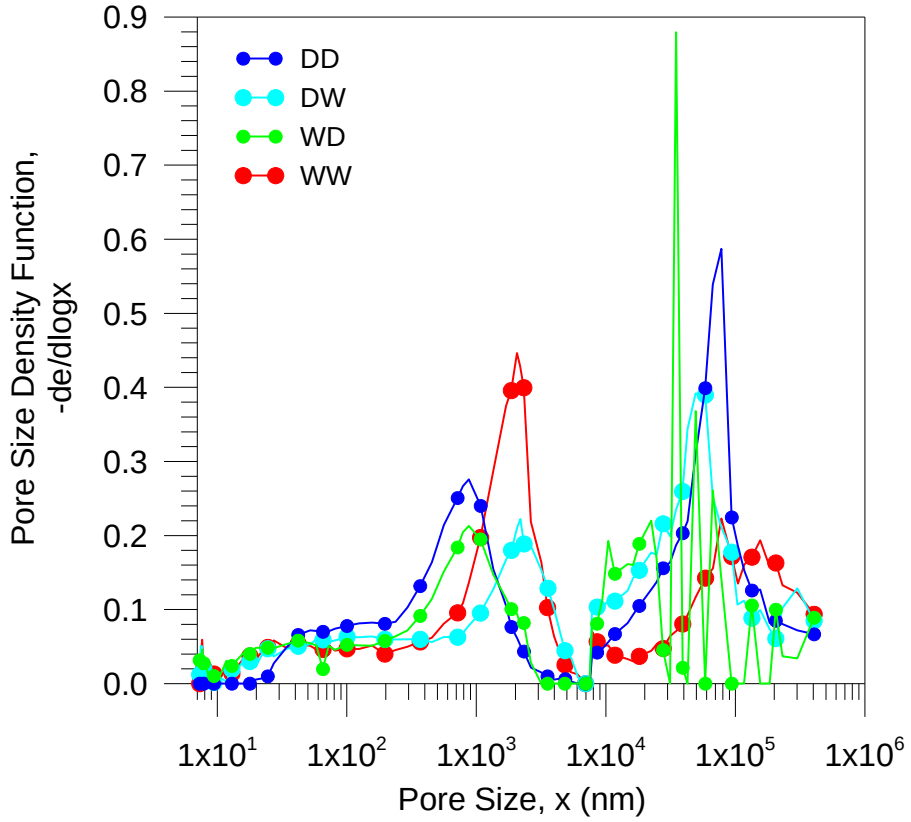

Figure 4.9: Complete porosimetry data

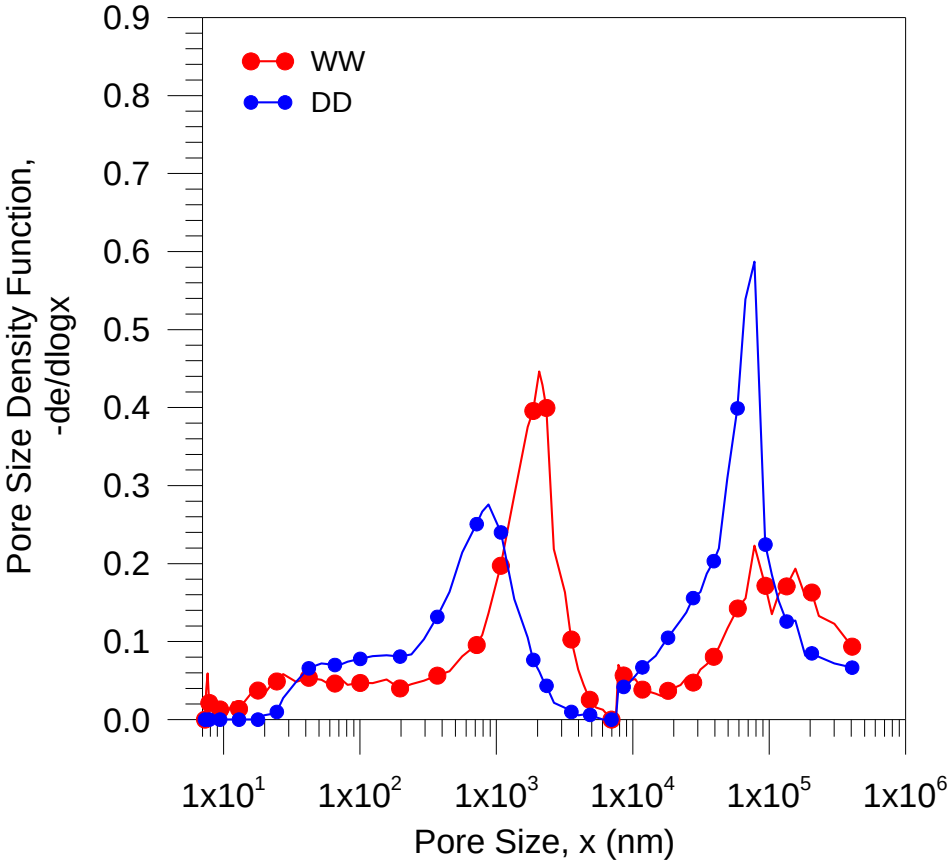

Figure 4.10: PSD data for WW against DD

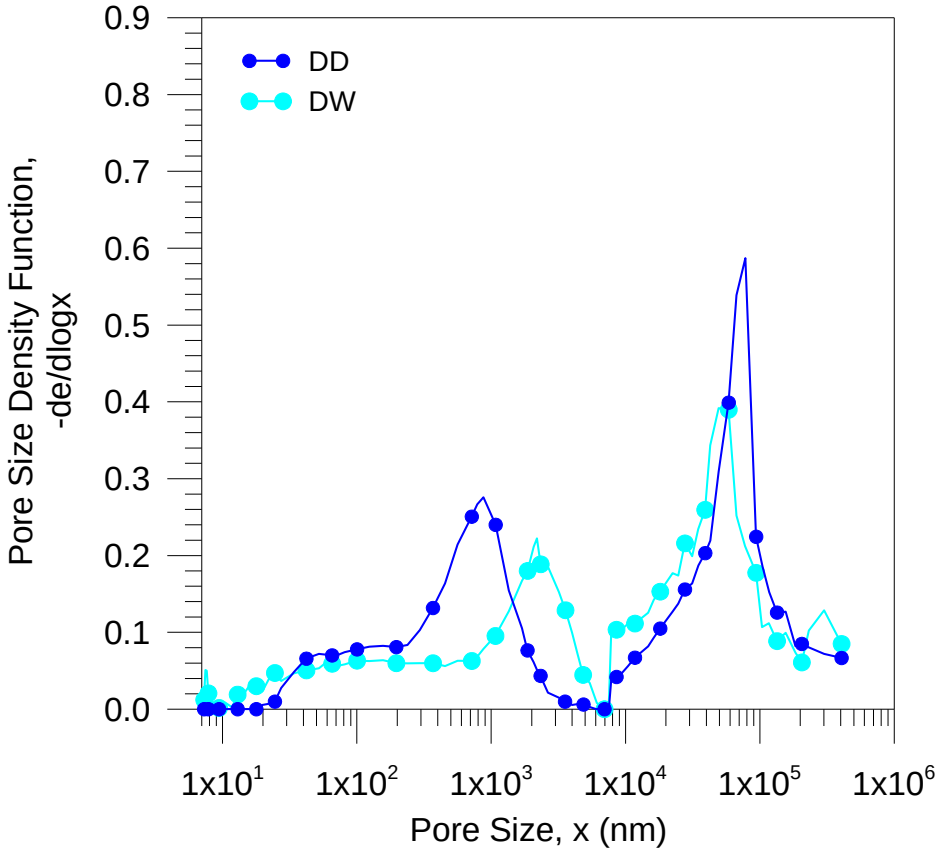

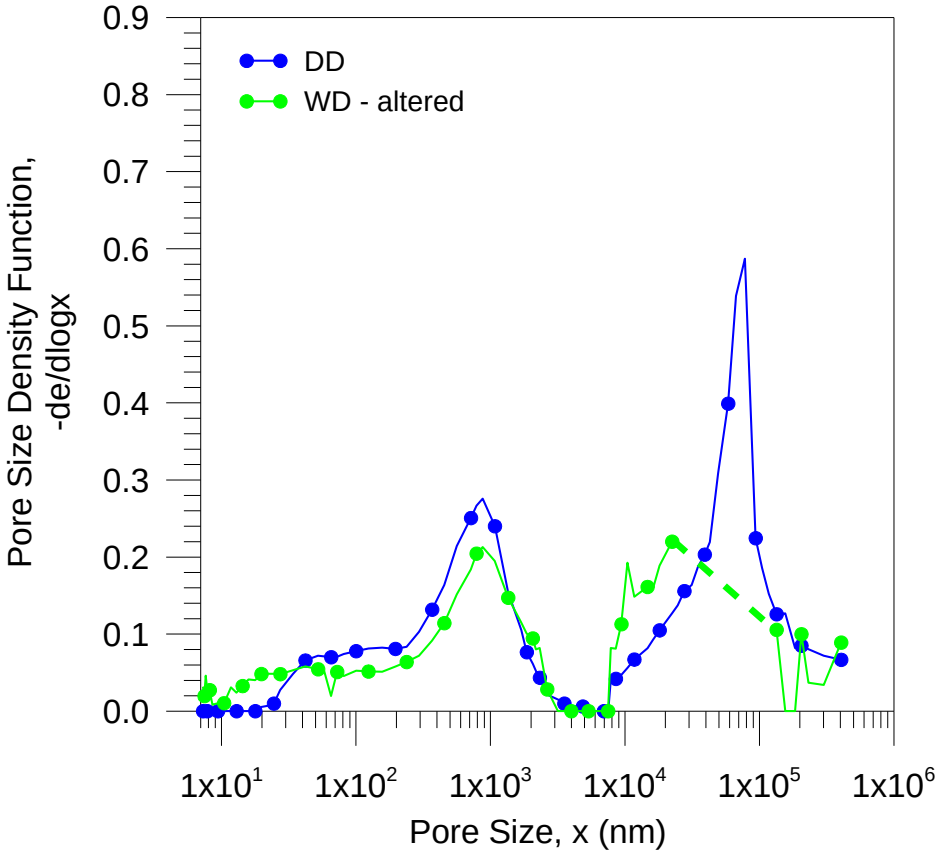

Figure 4.11: Comparison of (a) DD and DW (b) DD and altered WD pore size distributions

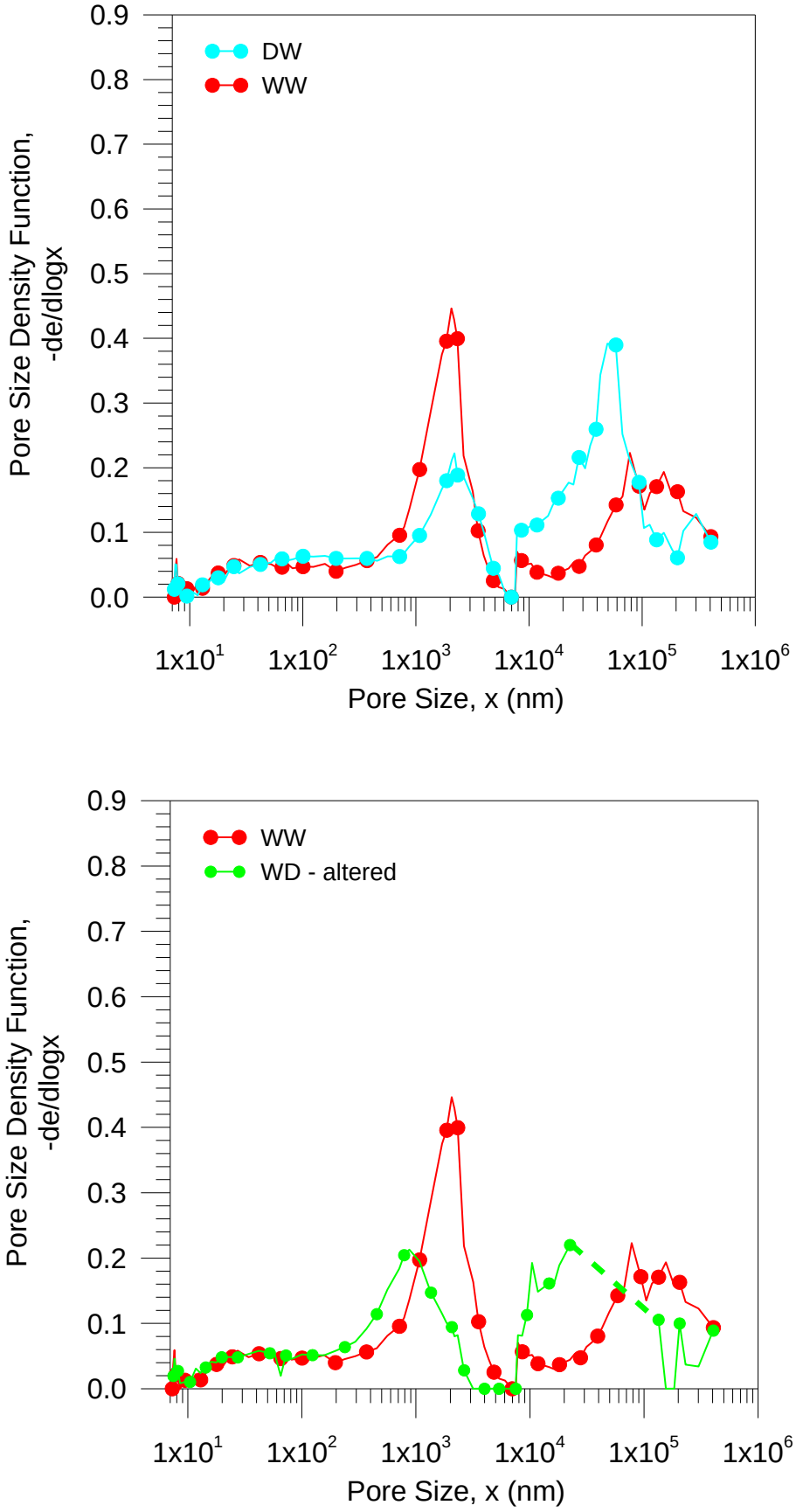

Figure 4.12: Comparison of (a) WW and DW (b) WW and WD pore size distributions

4.5. Retention Curves

4.5.1. MIP

The retention curves as shown in Figure 4.13 show again that the behaviour of the soil is dependent on the water content at compaction, with strong similarities between the retention curves of DD and DW samples and those of the WW and WD samples as shown in Figure 4.15.

We can see from that the behaviour is mainly controlled by the inter-aggregate forces, with only a small section of high suction values controlled by intra-aggregate forces (Romero et al., 1999). We can see this using the delimiting values shown earlier, which correspond to values of suction of around 2MPa for the dry samples and 5MPa for the wet samples.

There is an increased value of suction for given water content in the WW and WD samples, this is due to the different microstructures produced during compaction. The wet samples present a matrix type structure (Alonso et al., 1987) providing stronger inter-aggregate forces between particles whereas those compacted on the dry side present with aggregate or clay connector structures which provide weaker inter-aggregate forces.

As the suction becomes controlled by intra-aggregate forces, the curves diverge, with total suction becoming insensitive to degree of saturation changes (changes in water content) due to macro-porosity reduction upon mechanical loading (Romero et al., 1999).

We can also see that for high levels of humidity and low levels of suction (below 100kPa), i.e. approaching fully saturated, the retention properties become entirely dependent on water content, not microstructure. This highlights the differences in behaviour between partially and fully saturated soils and hence the importance of microstructure in partially saturated soils.

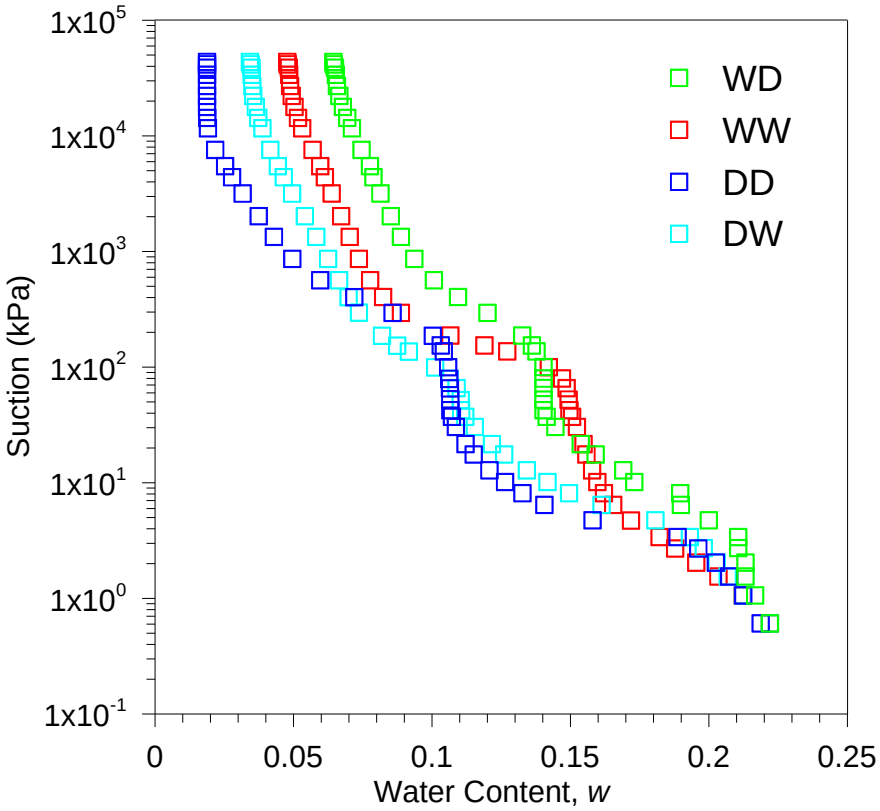

Figure 4.13: Complete MIP retention curve data

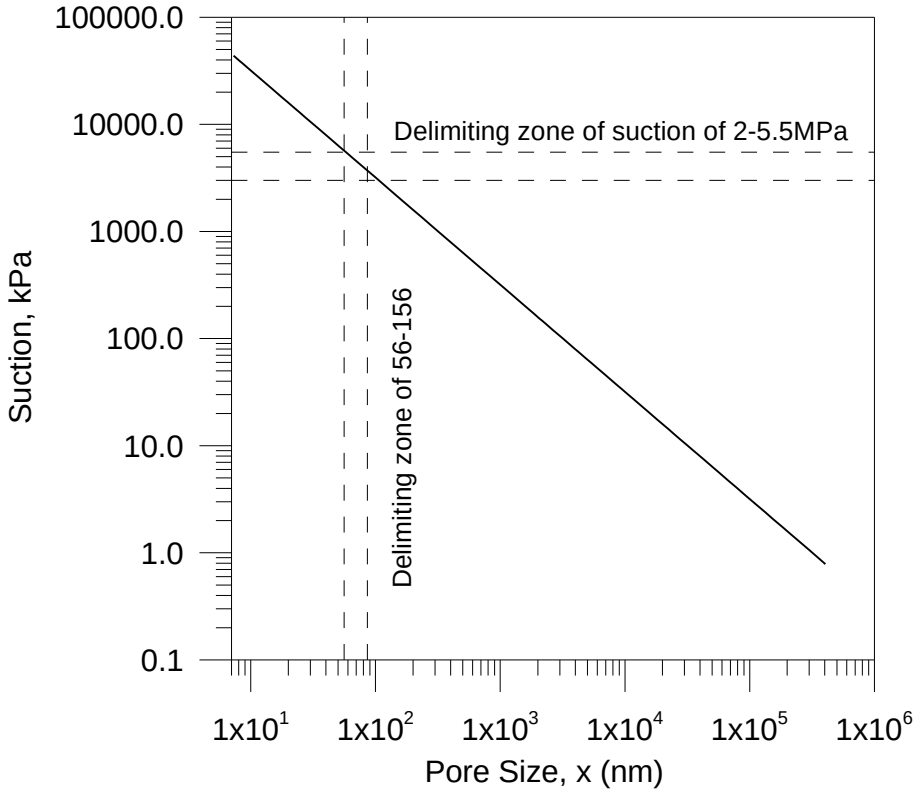

Figure 4.14: Derivation of delimiting values of suction

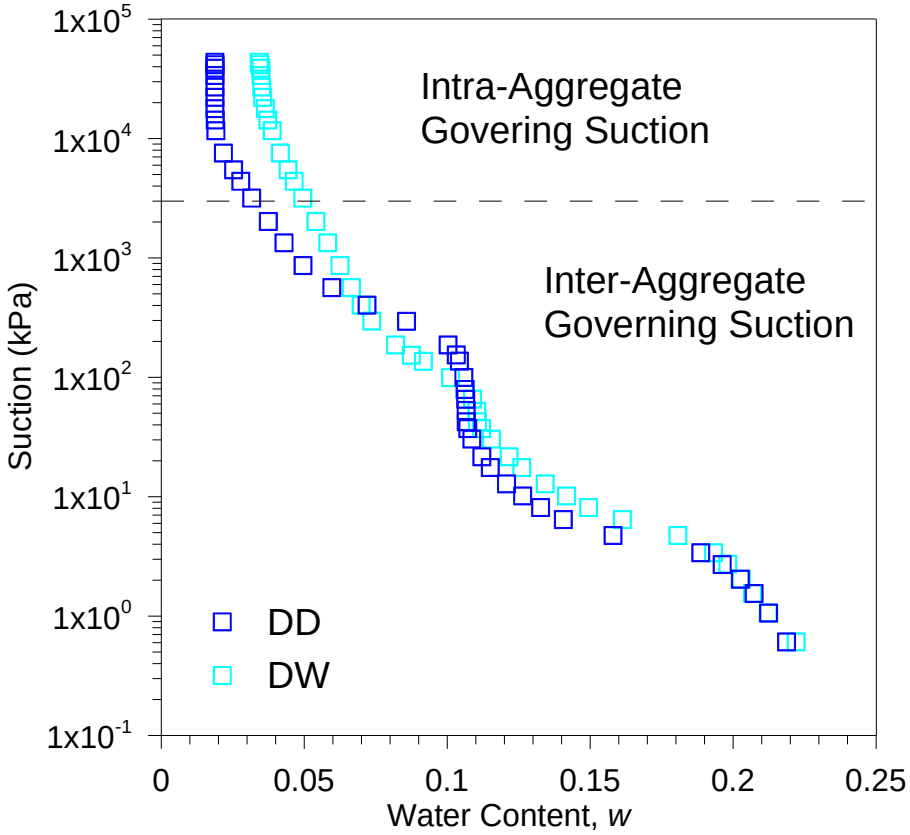

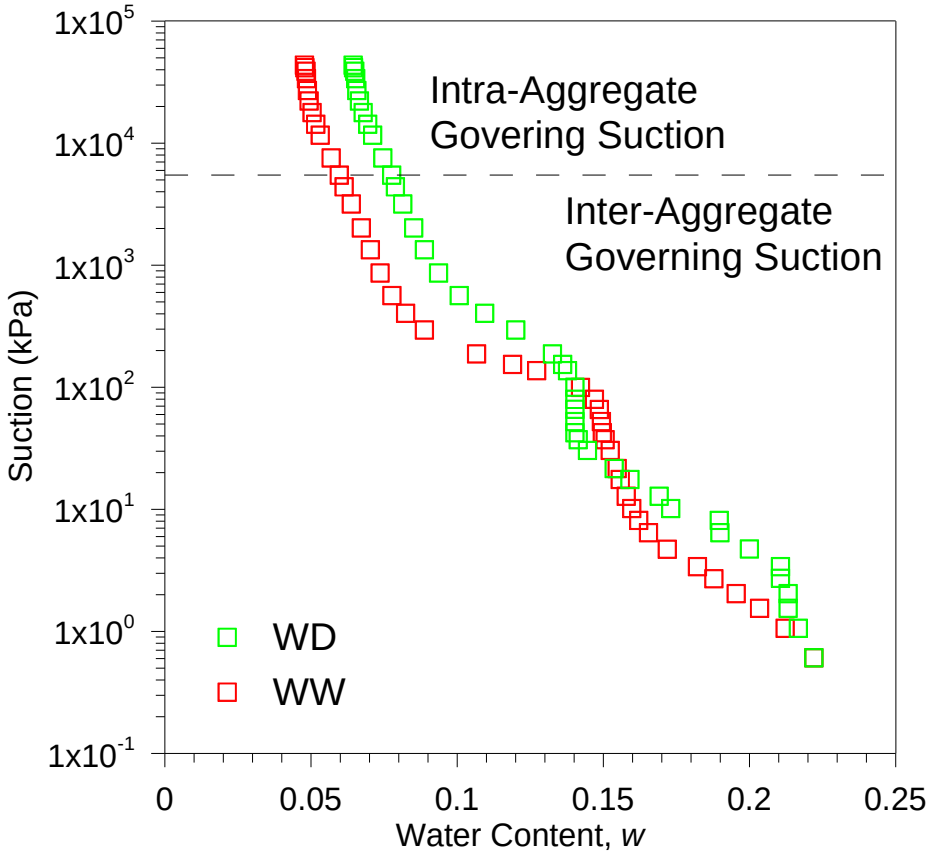

Figure 4.15: Comparision of (a) DD and DW and (b) WW and WD retention curves

4.5.2. WP4

If the results higher levels of suction obtained using the WP4 are plotted with lower value of suction obtained through the MIP as shown in Figure 4.16, we can see the results are consistent.

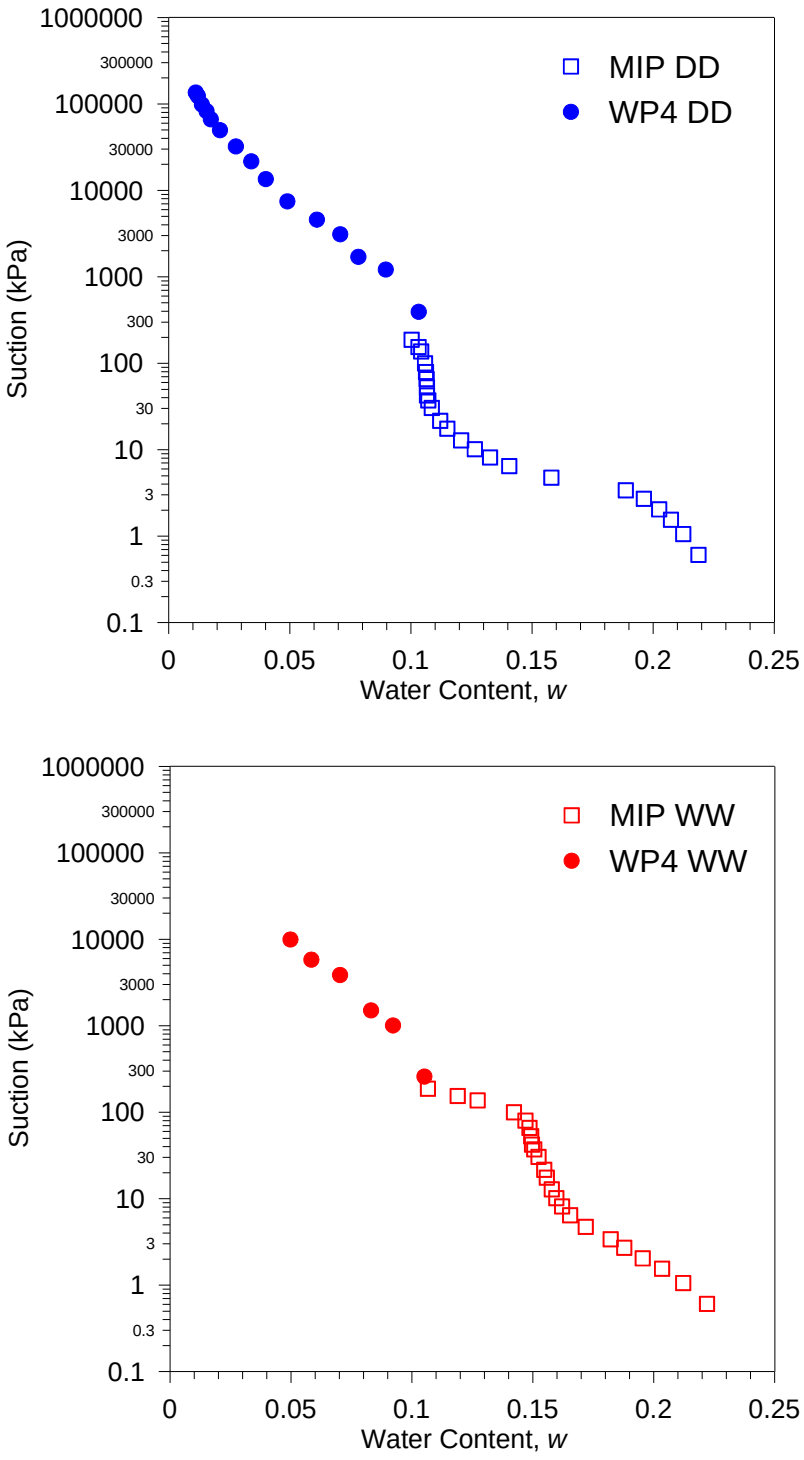

Figure 4.16: WP4 retention curve data with MIP data for (a) DD and (b) WW samples

4.6. Resonant Column Tests

Table 4.6: Complete results from resonant column experiments

Sample	$(\gamma_d)_0$	w_o	G_s
DD	1.684	12.13%	51.8
DD2	1.691	11.70%	34.0
DW	1.679	19.00%	8.1
DW2	1.679	18.42%	34.4
WD	1.679	12.29%	76.7
WD2	1.690	13.93%	69.1
WD3	1.679	12.38%	56.4
WW	1.678	17.52%	33.8
WW2	1.747	16.75%	17.4

Table 4.6 shows the full set of experimental results from the resonant column experiments conducted. However, some samples were not representative for a number of reasons. Sample DW presented an abnormally low value of G_s which is probably due to equipment problems, namely the screws attaching the coils to the sample were not tight, resulting in a skewed measurement. Sample WW2 was compacted at too high a dry density making it incomparable to the other samples. Samples WD2 and DD2 were compacted at too high and low a water content respectively to be comparable.

Omitting the above samples, samples DD, DW2, WD, WD3, and WW will be used for comparison. Figure 4.17 shows the wetting and drying paths these samples were subjected to.

In sample DW2 two sets of readings were taken, in the first, the experiment had not yet equilibrated however in the second, the sample was left overnight and dried to 15.96%. As neither of these results are representative, an average of the two has been used.

The results shown in Figure 4.18 clearly show that dry samples have higher value of G_s than wet samples. With the results obtained, it would be difficult to comment definitively on the effect of the wetting and drying on the value of G_s, especially with the uncertainty of the DW2 sample, although it is clear that samples that were dried have a higher rigidity than those compacted dry whereas there is much less if not no change in G_s between the WW and DW samples.

This behaviour leads us to examine to the effect of saturation on the rigidity. The values of rigidity and saturation are shown in Table 4.7 and plotted in Figure 4.19. Assuming sample DW (circled) is anomalously high, perhaps to experimental error, the figure clearly shows a peak in G_s at a degree of saturation of 0.645.

Table 4.7: Comparision of Gs and Sr

Sample	G	Sr
DD	51.8	0.54
DD2	34.0	0.53
DW	8.1	0.84
DW2	34.4	0.82
WD	76.7	0.55
WD2	69.1	0.63
WD3	56.4	0.55
WW	33.8	0.78
WW2	17.4	0.83

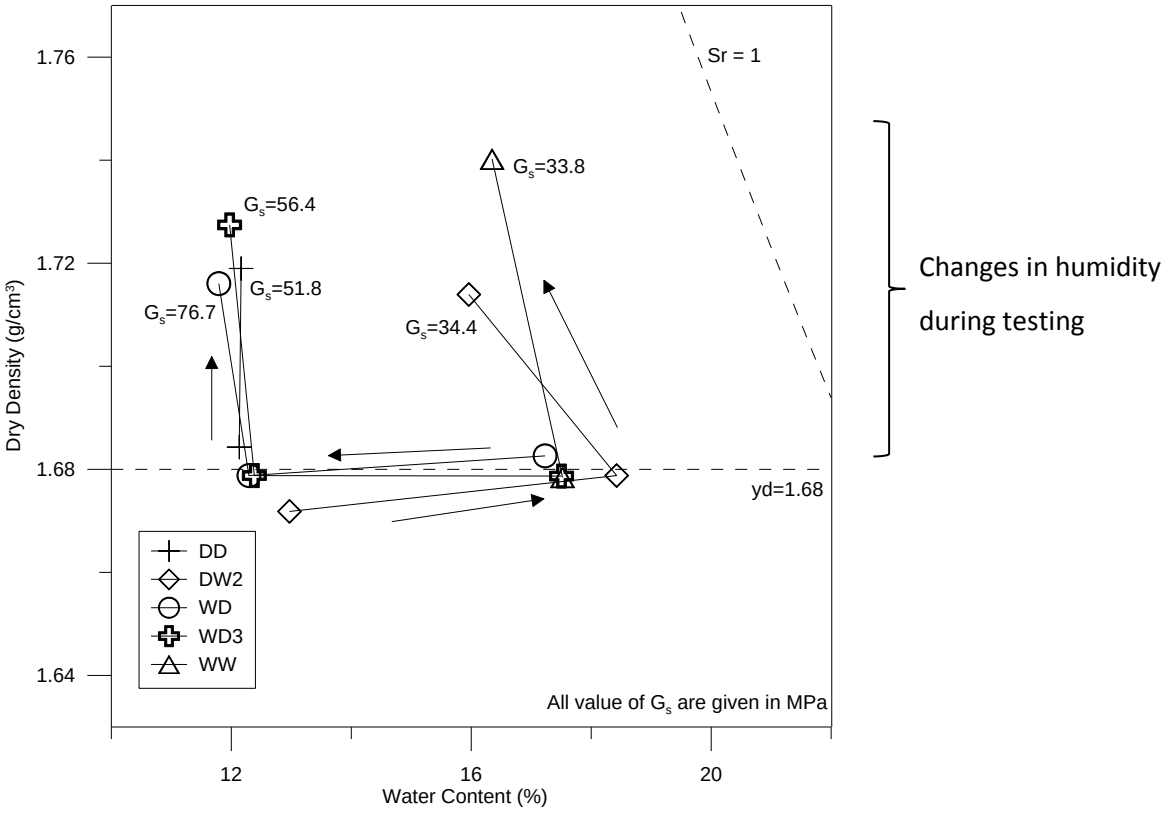

Figure 4.17: Wetting and drying paths of samples

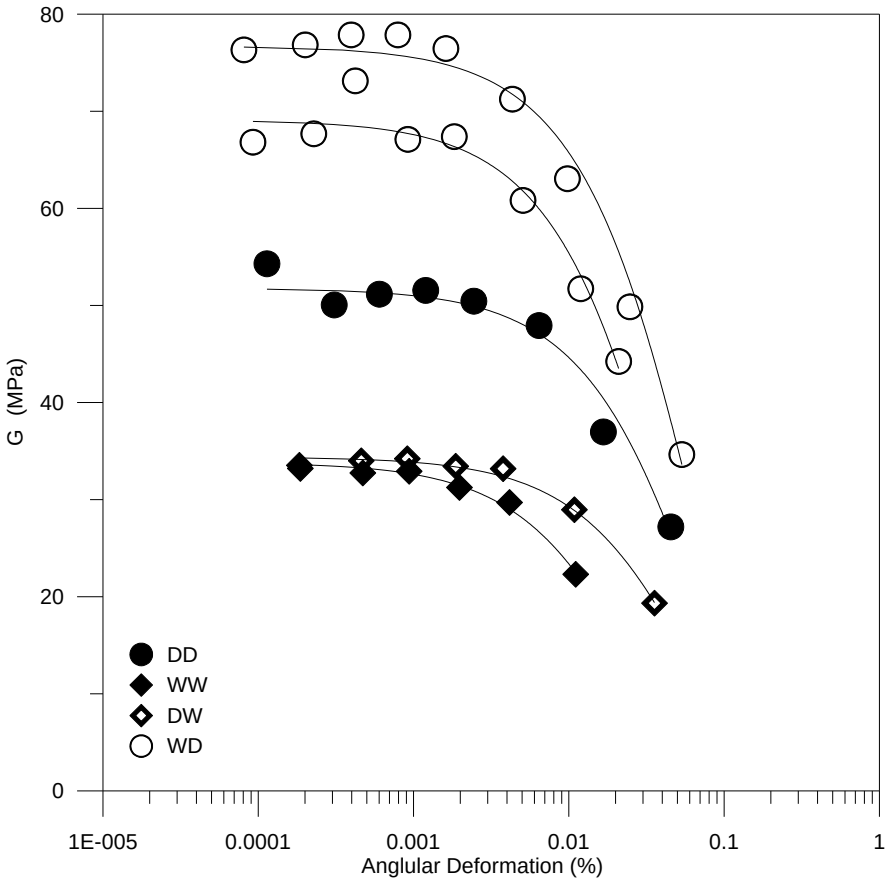

Figure 4.18: Resonant column results for Gs

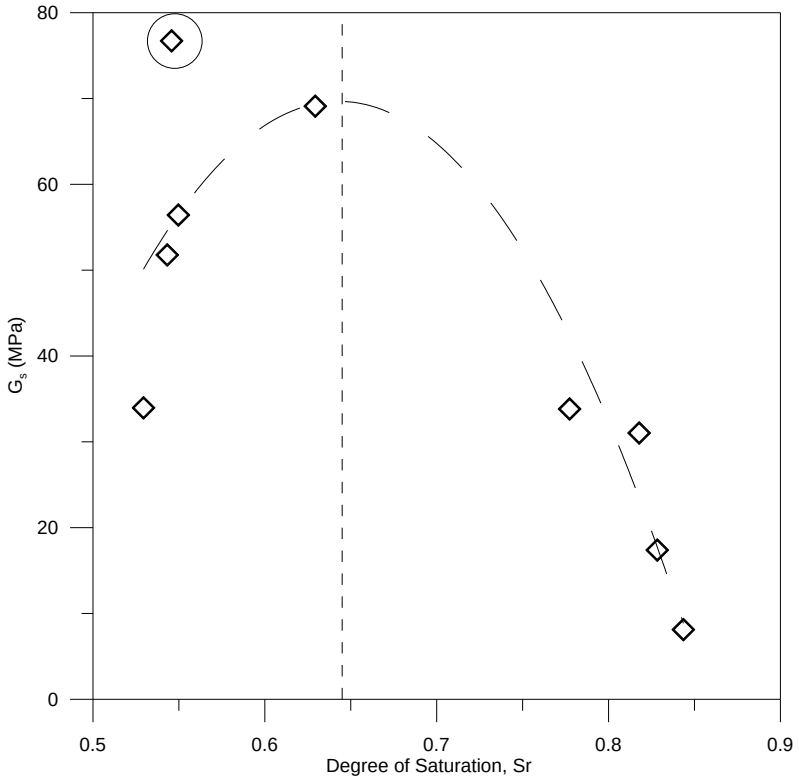

Figure 4.19: Comparison of Gs and Sr

4.7. Oedometer Tests

Table 4.8: Sample data of suction controlled oedometer tests

Sample	*w* at compaction	*w* at start of test	Compaction Path
DD-20	12.66%	12.66%	A
DD-400	12.83%	12.83%	B
WD-400	17.51%	12.23%	B

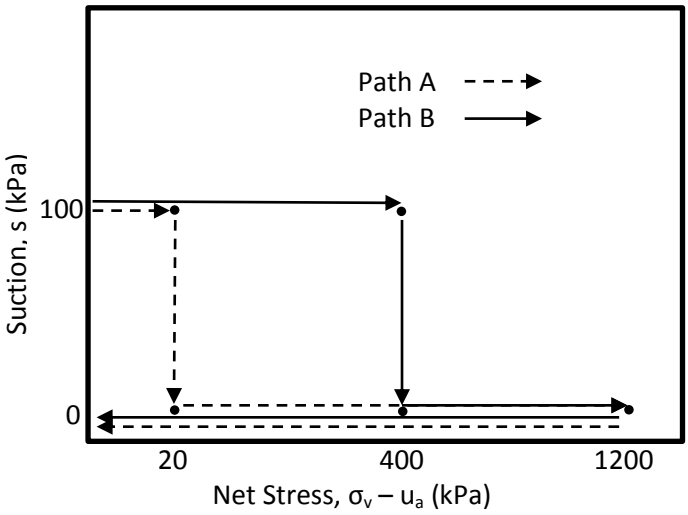

Figure 4.20: Oedometric loading paths

Figure 4.20 shows the loading and unloading paths of the three samples tested in the suction controlled oedometer and Figure 4.22 shows the evolution of the void ratio with net stress. If we compare the two samples compacted to 400kPa, DD and WD, we can see a difference in the loading paths, with the WD sample having a much lower void ratio during loading but the DD sample presenting a much steeper drop in e but once flooded the two samples behaved almost identically during unloading.

Comparing the deformation of the samples with net stress, we see some distinct differences between the WD and DD samples. The WD-400 sample and the DD-400 sample show the same path shape but the WD-400 sample shows distinctly less deformation overall than either the DD-20 or the DD-400. This again shows the effect of the microstructure of the behaviour of the soil, sample WD-400 which was compacted on the wet side showing reduced capacity for compression. However, the stiffness of all three samples is very similar especially after flooding. We can see that the stiffness during unsaturated compaction is more constant in the WD-400 sample than the DD-400 sample.

Looking at compressibility, $^{\delta e}/_{\delta log \sigma_v}$ we can see that after flooding and during unloading, these are almost identical for the three samples, but that the compressibility in the unsaturated stage is greater in the DD-400 than in unloading; similarly but to a lesser extent in the WD-400 sample.

As suction goes to 0, the response from the DD-400 sample is much greater than the WD-400 sample. This behaviour can be shown as the effect of collapse is shown in Figure 4.21. The sample compacted on the wet side has less capacity for collapse due to a reduction in large inter-aggregate pore spaces. During unloading the slope of all three samples are very similar, with the slight divergence of the DD-400 attributed to gaps in sampling due to that section of the experiment being overnight.

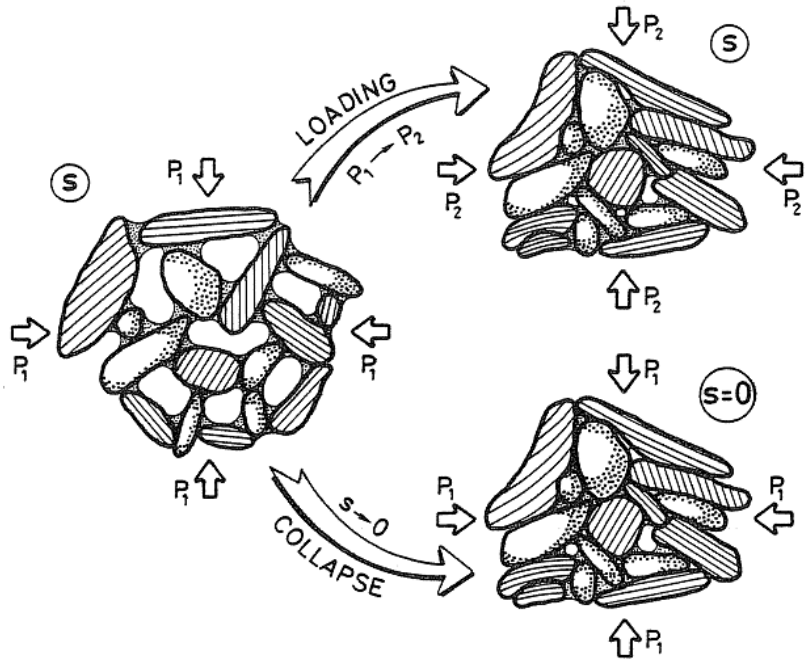

Figure 4.21: Microstructural interpretation of loading and collapse deformations (Alonso et al., 1990)

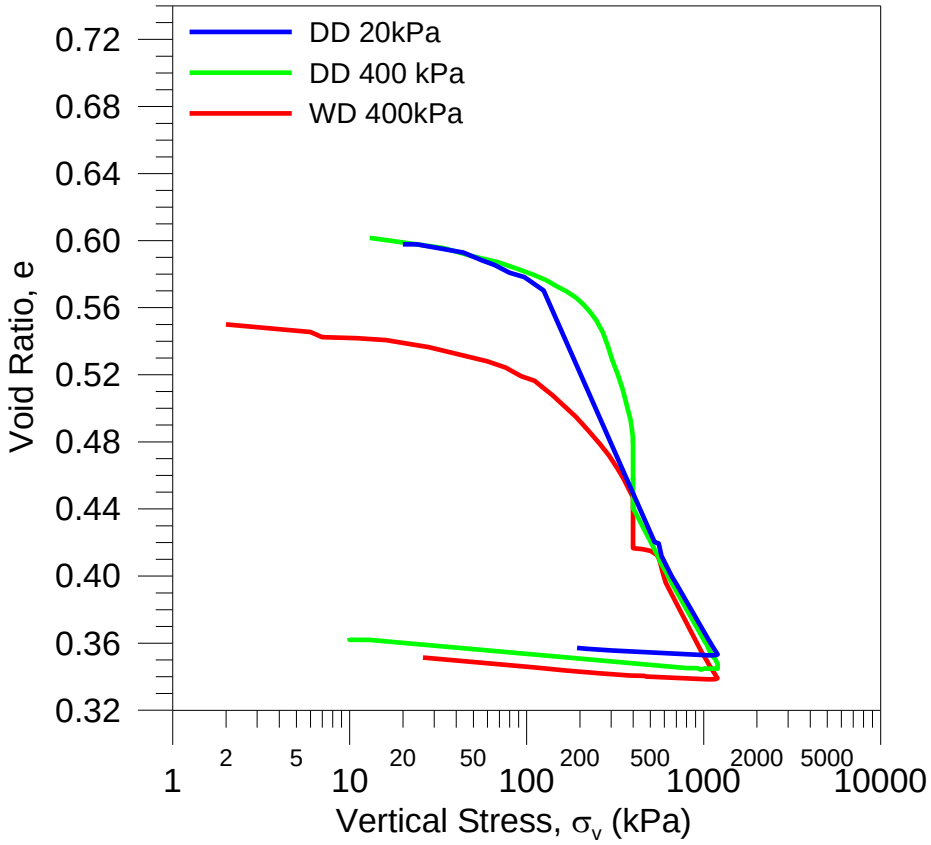

Figure 4.22: Evolution of void ratio with net stress

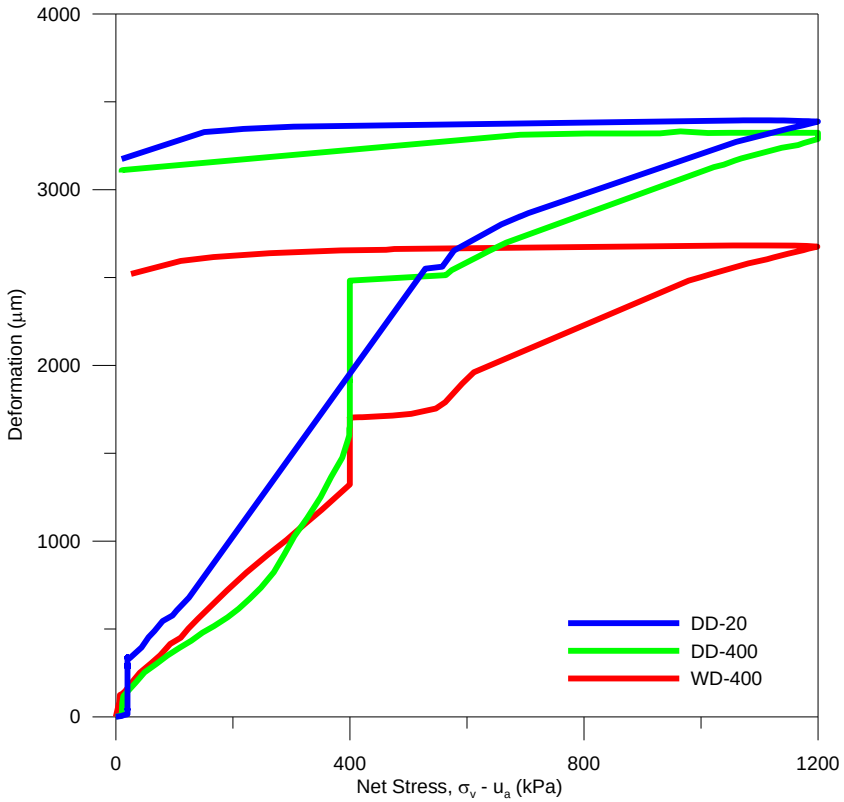

Figure 4.23: Deformation during loading and unloading

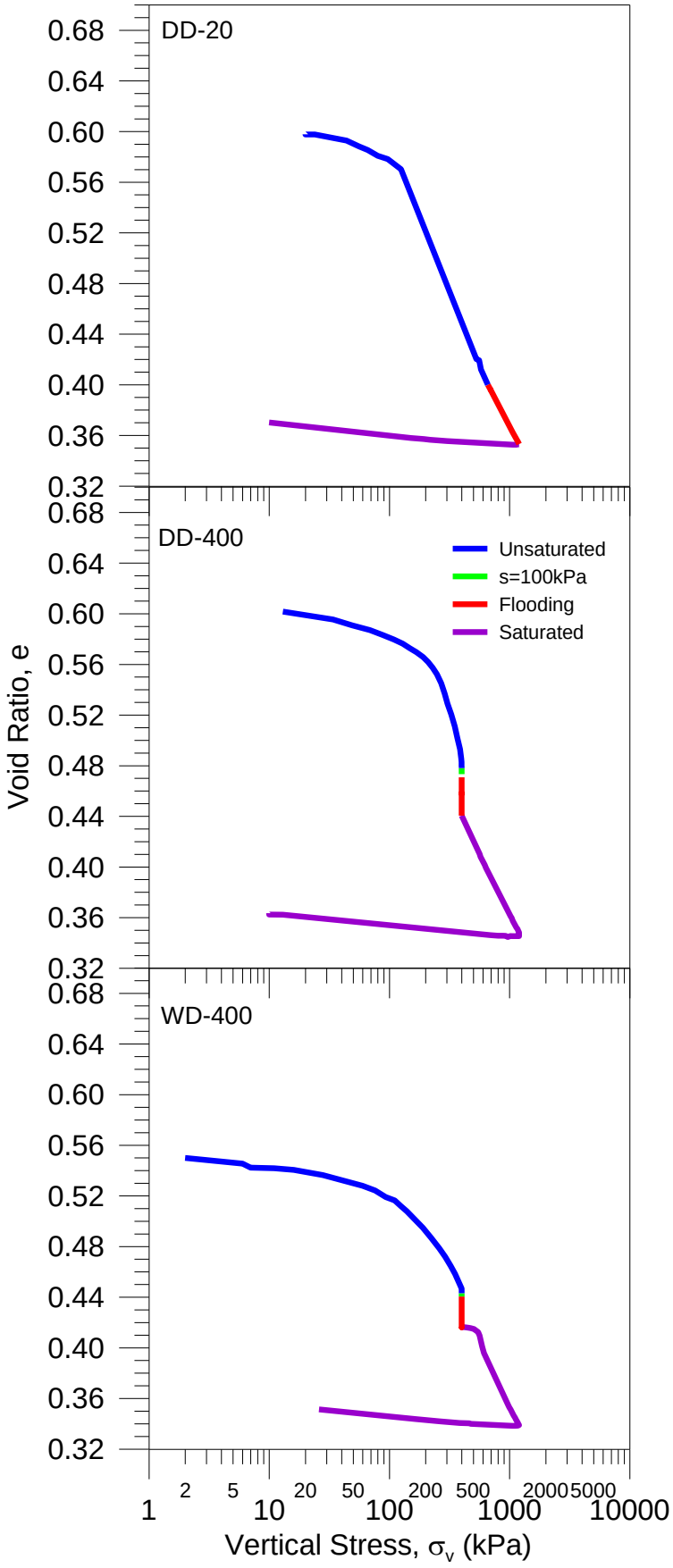

Figure 4.24: Changes in void ratio during stages of loading

5. Chapter 5 – CONCLUSIONS AND POSSIBLE FURTHER LINES OF INVESTIGATION

The results presented in chapter 4 show that volumetric behaviour is largely dependent on conditions during compaction. However, some characteristics on both a micro and global scale are effected by wetting and drying cycles.

The results of the classification tests showed the sample to be a fairly well graded low plasticity silty-clay; this is consistent with the behaviour demonstrated in the following experiments.

- The pore size distributions are generally consistent with previous findings of Gens et al. (1995) and Suriol (2007) with a more bimodal distribution apparent in samples compacted on the dry side and a more prominent single peak for those compacted on the wet side although the WD sample tended more towards a bi-modal distribution that the WW sample, showing an effect in the microstructure of the drying process.

- Intrusion and extrusion data presented a clear picture of a microstructure determined by the water content at compaction in intermediate value of suction but little dependence in values of suction below 100kPa.

- The theories of Delage and Lefebvre (1984) of inter- and intra- aggregate governing regions are consistent with the results of the retention curve data with the values of suction in the intra-aggregate governing region showing little to no dependence on water content of the sample.

- An increase in e_{micro} was observed in those samples compacted at higher water content but little correlation with the humidity at testing.

- Results of the suction controlled oedometer tests show that the level of deformation of the sample is entirely controlled by the water content at compaction with the WD sample showing much lower collapsibility than the DD samples. However, stiffness and compressibility during loading after saturation and unloading is unaffected by the compaction conditions.

- The resonant column tests showed strong correlation of rigidity with water content at compaction with a clear increase in the rigidity from DD to WD samples although there is no clear correlation with the WW and DW samples. A bell shaped relationship between degree

of saturation and rigidity was also observed with an apparent peak at around a saturation of 0.645.

- Overall, the above data shows that some changes in microstructure can be observed during wetting and drying with no overall volumetric change however that in the majority of experiments the noted behaviour was more reliant on sample conditions during compaction, not conditions during testing.

Possible further lines of investigation could include triaxial testing to determine changes in permeability with samples subjected to wetting and drying. Testing DW and WD samples that have experienced no volume change against DD and WW samples, would enhance the picture of changes within the microstructure during wetting and drying.

A comparison with a study of the same soil that was wetted and dried with changes to the dry density, could demonstrate the extent to which swelling and shrinking, macrostructural changes, have on soil behaviour against microstructural changes.

Tests to observe any development of anisotropic behaviour with wetting and drying could yield information about particle arrangement within the microstructure of the soil.

Also, The use of SEM photos would help to reinforce some of the ideas put forward about changes in microstructure during volume controlled wetting and drying.

6. Chapter 6 – REFERENCES

Ahmed, S., Lovell, C. W.,Jr. & Diamond, S. (1974) Pore sizes and strength of compacted clay. *Journal of the Geotechnical Engineering Division, ASCE,* 100 (GT4), 407-425.

Alonso, Eduardo. Suelos Compactados en la Teoría y en la Práctica. *Catedrático De Ingeniería Del Terreno,* November 2007.

Alonso, E.E., Gens, A., and Hight, D.W. (1987) Special problem soils. General report. In proceedings of the 9th European Conference on Soil Mechanics and Foundation Engineering, Dublin, Vol. 3: 1087-1146.

Alonso, E. E., Gens, A. & Josa, A. (1990) A Constitutive Model for Partially Saturated Soils. *Geotechnique,* 40 (3), 405-430.

Alonso, E. E., Pereira, J. -M, Vaunat, J. & Olivella, S. (2010) A microstructurally based effective stress for unsaturated soils. *Geotechnique,* 60 (12), 913-925.

Alonso, E. E., Romero, E. & Hoffmann, C. (2011) Hydromechanical behaviour of compacted granular expansive mixtures: experimental and constitutive study. *Geotechnique,* 61 (4), 329-344.

Alonso, E. E., Vaunat, J. & Gens, A. (1999) Modelling the mechanical behaviour of expansive clays. *Engineering Geology,* 54 (1-2), 173-183.

Alonso, Eduardo E., Pinyol, Núria M., Puzrin, Alexander M., (2010) *Collapse of Compacted Soil: Girona Road Embankments, Spain.* Geomechanics of Failures. Advanced Topics, Springer Netherlands.

Aitchison, G.D. and Bishop, A.W. (1960). Discussion in Pore pressure and suction in soil. 150. London: Butterworths.

Barden, L. (1974) Consolidation of Clays Compacted Dry and Wet of Optimum Water-Content. *Geotechnique,* 24 (4), 605-625.

Barrera Bucio, Mauricio. (2002) *Estudio experimental del comportamiento hidro-mecánico de suelos colapsables, Tesis Doctoral.*

Bishop, A.W. and Blight, G.E. (1963). Some aspects of effective stress in saturated and unsaturated soils. Géotechnique 13, No 3: 177-197.

Blatz, J. A., Graham, J. & Chandler, N. A. (2002) Influence of suction on the strength and stiffness of compacted sand-bentonite. *Canadian Geotechnical Journal,* 39 (5), 1005-1015.

Booth A.R. (1977). Collapse Settlement in Compacted Soils. CSIR Research Report 324, NITRR Bulletin 13, Pretoria, South Africa.

British Standards. (2010) *BS EN 13286-2:2010: Unbound and hydraulically bound mixtures Part 2: Test methods for laboratory reference density and water content — Proctor compaction.*

Buenfil Berzunza, Carlos Manuel. (2007) *Caracterización experimental del comportamiento hidromecánico de una arcilla compactada.*

Cardoso, Rafaela. (2007) A Comparative Study of Soil Suction Measurement Using Two Different High-Range Psychrometers. (Part II), 79-93.

CRONEY, D. & COLEMAN, J. D. (1954) SOIL STRUCTURE IN RELATION TO SOIL SUCTION (pF). *Journal of Soil Science,* 5 (1), 75-84.

Das, B. M. & Ramana, G. V. (1993) Principles of Soil Dynamics [1st ed.], Cengage Learning, Stamford, CT.

Decagon Devices, Inc. (2011) *WP4 DewPoint Potentiameter, Overview.* [Online] Available from: http://www.decagon.com/products/discontinued-products/wp4-dewpoint-potentiameter/ .

Delage, P., Audiguier, M., Cui, Y. J. & Howat, M. D. (1996) Microstructure of a compacted silt. *Canadian Geotechnical Journal,* 33 (1), 150-158.

Delage, P. & Lefebvre, G. (1984) Study of the Structure of a Sensitive Champlain Clay and of its Evolution during Consolidation. *Canadian Geotechnical Journal,* 21 (1), 21-35.

Fredlund, D.G. (1979). Appropriate concepts and technology for unsaturated soils. Can. Geotech. J. 16 No 1: 121-139.

Gens, A., Alonso, E. E., Suriol, J. & Lloret, A. (1995) *Effect of structure on the volumetric behaviour of a compacted soil.* ROTTERDAM; PO BOX 1675, 3000 BR ROTTERDAM, NETHERLANDS, A A BALKEMA.

Gens, A., Vallejan, B., Sanchez, M., Imbert, C., Villar, M. V. & Van Geet, M. (2011) Hydromechanical behaviour of a heterogeneous compacted soil: experimental observations and modelling. *Geotechnique,* 61 (5), 367-386.

Georgiannou, V. N., Rampello, S. & Silvestri, F. (1991) *Static and Dynamic Measurements of Undrained Stiffness on Natural Overconsolidated Clays.* ROTTERDAM, A A BALKEMA PUBLISHERS.

Gómez, Rodrigo. (2009) *CARACTERIZACIÓN HIDRO-MECÁNICA DEL SUELO DEL TERRAPLÉN EXPERIMENTAL DE ROUEN*. Tesis de Master.

Lambe, T.W. (1958). The structure of compacted clay. Jnl. of the Soil Mech. and Foundn. Div ASCE, 84 (SM2): 10-34.

Lambe, T.W. and Whitman, R.V. (1959). The role of the effective stress in the behaviour of expansive soils. Quart. Of the Colo. Sch. Of Mines, Vol. 54 (4): 33-66

Leong, E. C., Tripathy, S. & Rahardjo, H. (2003) Total suction measurement of unsaturated soils with a device using the chilled-mirror dew-point technique. *Geotechnique,* 53 (2), 173-182.

Lo Presti, D. C. F., Jamiolkowski, M., Pallara, O., Cavallaro, A. & Pedroni, S. (1997) Shear modulus and damping of soils. *Geotechnique,* 47 (3), 603-617.

Marinho, F., Take, W. & Tarantino, A. (2008) *Measurement of Matric Suction Using Tensiometric and Axis Translation Techniques.* Springer Netherlands.

Matyas, E.L. and Radhakrishna, H.S. (1968). Volume change characteristics of partially saturated soils. Géotechnique, 18, No 4: 432-448.

Mills, K. G. and Cameron, D. A. (2002). Engineering Soil Classification. Accessed from: www.unisanet.unisa.edu.au.

Murray, E. J. & Sivakumar, V. (2010) *Unsaturated soils: a fundamental interpretation of soil behaviour.* Ames USA, Wiley-Blackwell.

Pineda, J. A., Romero, E. E. & Colmenares, J. E. (2008) *Suction effects on the pre-failure behaviour of a compacted clayey soil.* BOCA RATON; 6000 BROKEN SOUND PARKWAY NW, STE 300, BOCA RATON, FL 33487-2742 USA, CRC PRESS-TAYLOR & FRANCIS GROUP.

Poulovas.a & Tzimas, E. (1974) Hysteresis in Relationship between Hydraulic Conductivity and Suction. *Soil Science,* 117 (5), 250-256.

Proctor, R. R. (1933) Fundamental principles of soil compaction. *Engineering News-Record,* 111 (13), 372.

Richart, F. E., Hall, J. R. & Woods, R. D. (1970) *Vibrations of Soils and Foundations.* New Jersey, Prentice-Hall Inc.

Romero, E. (1999). Thermo-hydro-mechanical behaviour of unsaturated Boom clay: an experimental study. Ph. D. Thesis, Technical University of Catalunya, Barcelona.

Romero, E. & Vaunat, J. (2000) Retention curves of deformable clays. In: Tarantino, A. & Mancuso, C. (eds.) *Experimental Evidence and Theoretical Approaches in Unsaturated Soils.* Rotterdam, AA. Balkema, pp. 91-106.

Romero, E., Gens, A. & Lloret, A. (1999) Water permeability, water retention and microstructure of unsaturated compacted Boom clay. *Engineering Geology,* 54 (1-2), 117-127.

Romero, Enrique & Simms, Paul H. (2009) *Microstructure Investigation in Unsaturated Soils: A Review with Special Attention to Contribution of Mercury Intrusion Porosimetry and Environmental Scanning Electron Microscopy.* Laboratory and Field Testing of Unsaturated Soils, Springer Netherlands.

Simms, P. H. & Yanful, E. K. (2004) A discussion of the application of mercury intrusion porosimetry for the investigation of soils, including an evaluation of its use to estimate volume change in compacted clayey soils. *Geotechnique,* 54 (6), 421-426.

Sivakumar, V., Sivakumar, R., Murray, E. J., Mackinnon, P. & Boyd, J. (2010) Mechanical behaviour of unsaturated kaolin (with isotropic and anisotropic stress history). Part 1: wetting and compression behaviour. *Geotechnique,* 60 (8), 581-594.

Suriol i Castellvi, Josep. (1993) Medida de la deformabilidad de suelos mediante el equipo de columna resonante. *Revista De Obras Públicas,* 3319, 57-66.

Suriol, J., Gens, A. & Alonso, E. E. (1998) Beijing. Behaviour of Compacted Soils in Suction-Controlled Oedometer. 137, Chaonei Dajie, Beijing 100010, People's Republic of China, International Academic Publishing House.

Suriol, Josep & Lloret, Antoni. (2007) Cambios en la Estructura de Suelos Compactados Frente a Humedecimiento y Secado. *Ingeniería Civil,* 147, 67-78.

Taibi, S., Fleureau, J. M., Abou-Bekr, N., Zerhouni, M. I., Benchouk, A., Lachgueur, K. & Souli, H. (2011) Some aspects of the behaviour of compacted soils along wetting paths. *Geotechnique,* 61 (5), 431-437.

Tarantino, A. (2007) A possible critical state framework for unsaturated compacted soils. *Geotechnique,* 57 (4), 385-389.

Tarantino, A. & De Col, E. (2008) Compaction behaviour of clay. *Geotechnique,* 58 (3), 199-213.

Yenes, Mariano, Nespereira, José, Blanco, José, Suárez, Mercedes, Monterrubio, Serafín & Iglesias, Carlos. (2010) *Shallow foundations on expansive soils: a case study of the El Viso Geotechnical Unit, Salamanca, Spain.* Springer Berlin / Heidelberg.